

Power Law Behavior in the Spatial and Frequency Domain Governing Thermal Slip at a Liquid/Solid Interface

Hiroki Kaifu and Sandra M. Troian*

California Institute of Technology

T. J. Watson Sr. Laboratories of Applied Physics

Pasadena, CA 91125

(Dated: May 14, 2025)

Integrated chips for power intensive graphics and computer processing applications dissipate so much heat nowadays that liquid based cooling has become practically essential to prevent breakdown from thermal runaway. Fortunately, cooling schemes based on immersion technology or microfluidic networks are proving effective. However, further progress ultimately requires tackling the intrinsic thermal impedance caused by the discontinuity in properties across the liquid/solid (L/S) interface. Since experimental tools still lack sufficient spatiotemporal resolution for this purpose and given there are no analytic models for phonon propagation across the L/S interface, researchers have come to rely heavily on non-equilibrium molecular dynamics (NEMD) simulations. The goal of this computational study was to determine whether there exist compact general equations for the thermal slip length based on correlated behavior in the L/S contact zone. The results reveal power law equations for the thermal slip length incorporating the influence of molecular interaction parameters, local temperature, long range translational order and peak vibrational frequencies. These findings offer a promising route forward directed at the influence of surface localized phonons in the L/S contact zone.

I. INTRODUCTION

High performance GPUs and CPUs for extensive data mining required by applications like artificial intelligence and cryptocurrency exchange generate such tremendous heat within such small volumes that chip designers have had to pivot from air to liquid cooling to prevent operational failure [1–3]. This switch has pioneered faster clock speeds and higher efficiency, performance and stability in many systems, ranging from conventional CMOS and superconducting processors to solid-state quantum devices [4]. Despite well optimized cooling schemes however, there still remains the ultimate challenge of minimizing the intrinsic thermal impedance associated with any material interface, including liquid/solid (L/S) interfaces. And as integrated chips become smaller and smaller, now approaching nanoscale dimensions, the ratio of surface to volume thermal resistance therefore undergoes a substantial increase. For certain L/S systems at very low temperature, namely superfluid/metal interfaces, there do exist two analytic expressions for estimating the thermal boundary resistance [5–7] - better known as the Kapitza resistance - depending on whether the phonon transmission at the interface is assumed to be purely specular or purely diffusive. However, given that there is yet no general phonon theory for normal liquids, no comparable models exist for L/S systems at non-cryogenic temperatures.

This issue poses a fundamental problem since the temperature boundary condition needed for solving the continuum-level transport equation for heat crossing the

L/S interface remains unknown. Illustrated in Fig. 1 is the temperature jump ΔT in the L/S contact zone due to interfacial thermal resistance for a given thermal flux J_z propagating along the \hat{z} axis, oriented perpendicular to the L/S interface. The thermal boundary resistance is given by $\mathcal{R} = \Delta T/J_z$. In liquid/solid systems, it is more common to quantify this resistance by defining the so-called thermal slip length

$$L_T = \frac{\Delta T}{|dT/dz|_{liq}}, \quad (1)$$

where $|dT/dz|_{liq}$ is the magnitude of the thermal gradient within the liquid interior. While in macroscopic systems, the magnitude of ΔT is assumed to be negligibly small, such is not the case in micro- or nanoscale systems.

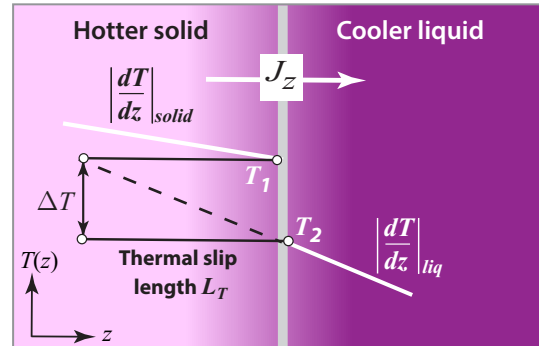


FIG. 1. Illustration of the thermal slip length $L_T = \Delta T/|dT/dz|_{liq}$.

A similar problem exists in fluid dynamics as well. The general velocity boundary condition (BC) at the L/S interface needed to solve Cauchy's momentum equation for a flowing liquid is also unknown. Unlike all the other BCs which can be used to solve transport equations in

* Corresponding author:
stroian@caltech.edu; www.troian.caltech.edu

hydrodynamics or heat transfer, neither the temperature nor velocity BC at the L/S interface can be derived from conservation laws or symmetry principles. NEMD simulations have therefore proven especially helpful in unveiling properties of the contact zone which help minimize the velocity slip length L_S . The systems examined have spanned a wide range, from simple to polymeric liquids to macromolecular solutions flowing across the surface of smooth, rough or patterned substrates [8–12]. Among other influences, it has been shown that L_S tends to exhibit a strong inverse dependence on the long range translational order within the first liquid layer induced by the substrate surface tension although the correct functional form has yet to be identified.

Over the past several decades, NEMD studies have uncovered correlations between the thermal slip length L_T and parameters such as the wettability of the L/S interface [13–18], bulk liquid pressure [19, 20], solid substrate temperature [21, 22], solid surface roughness features [18], solid lattice symmetry [23–25], thickness of the confined liquid layer [26], density depletion layer thickness [27–29] and more.

Such studies have examined the variation in L_T linked to changes in one or two parameters but even so, no general scaling has emerged. In recent work [25], we focused on structural properties of the L/S contact zone comprising the first adjacent solid and liquid layers. For simplicity, we refer to that liquid monolayer as the *contact layer*. Most importantly, that study revealed how 2D caged motion associated with in-plane restricted diffusion induced by the solid surface potential boosts thermal transport out-of-plane and across the L/S interface thereby reducing the thermal slip length. In this work, we identify power law relations in the spatial and frequency domain linking the thermal slip length to the long range translational order and peak frequency coupling across the L/S contact zone.

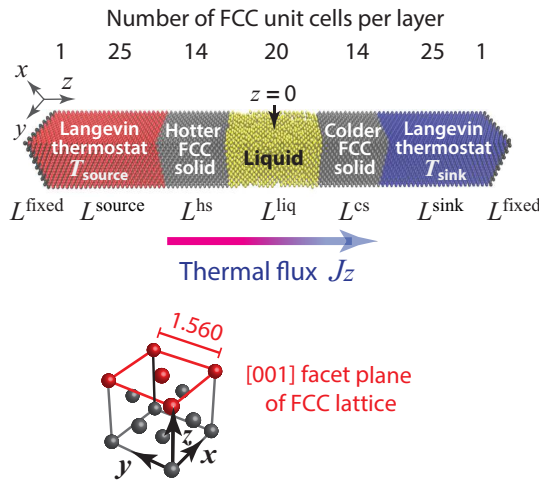


FIG. 2. Rectangular geometry showing number of FCC unit cells per layer. The surface normal to the [001] facet plane of each unit cell was oriented along the \hat{z} axis. Origin $z = 0$ was situated at the midplane of the liquid layer.

II. COMPUTATIONAL DETAILS

This section outlines details of the NEMD simulations conducted with open source software [30, 31]. Measurements supporting the findings are tabulated in the Appendix in Tables III through XI. The interested reader can find additional details in Ref. [25].

Physical quantity	Numerical value
mass	$m^* = 6.690 \times 10^{-26} \text{ kg}$
length	$\sigma^* = 0.3405 \times 10^{-9} \text{ m}$
energy	$\epsilon^* = 165.3 \times 10^{-23} \text{ J}$
temperature	$T^* = \epsilon^*/k_B = 119.8 \text{ }^\circ\text{K}$
time	$t^* = (m^* \sigma^{*2}/\epsilon^*)^{1/2} = 2.14 \text{ ps}$
mass density	$\rho^* = m^*/(\sigma^*)^3$
pressure	$p^* = \epsilon^*/(\sigma^*)^3 = 0.4187 \text{ MPa}$
effective particle diameters	$\sigma_{LL}^* = \sigma_{SS}^* = \sigma^*$ $\sigma_{LS}^* = 0.8, 1.0, 1.2 \sigma^*$
FCC edge length	$a^* = 1.560 \sigma^* = 5.312 \times 10^{-10} \text{ m}$
interaction energies	$\epsilon_{LL} = \epsilon^*$ $\epsilon_{LS} = 0.1 - 1.0 \epsilon^*$ $\epsilon_{SS} = 10 \epsilon^*$
Variable	Value in scaled units
solid & liquid particle mass	1.0
LJ repulsive distances	$\sigma_{LL} = \sigma_{SS} = 1.0$ $\sigma_{LS} = 0.8, 1.0 \text{ or } 1.2$
FCC edge length	$a = 1.560$
integration time step	$\Delta t_{int} = 0.002$
thermostat settings	$(T_{\text{source}}, T_{\text{sink}}) = (1.8, 0.8), (1.6, 1.0) \text{ or } (1.4, 1.2)$
LJ interaction energy	$\epsilon_{LL} = 1.0$ $\epsilon_{LS} = 0.1, 0.2, \dots, 0.9, 1.0$ $\epsilon_{SS} = 10$
bulk liquid density	$\rho_L \approx 0.84$
FCC unit cell density	$\rho_S = 1.0536$

TABLE I. Symbols, numerical values and scalings for non-dimensionalization of physical quantities based on fluid argon [32–34]. Superscripts with an asterisk denote dimensional quantities. Boltzmann's constant $k_B = 1.380649 \times 10^{-23} \text{ J/K}$.

A. Model

This study was based on the layered geometry in Fig. 2(a) and (b) consisting of a simple liquid sandwiched between two face-centered cubic (FCC) lattices, each in turn in thermal contact with an identical FCC lattice acting as a Langevin thermostat set to reservoir temperatures T_{source} and T_{sink}). The final layer of particles in the peripheral regions (L^{fixed}) were affixed in place to prevent migration beyond the edges of the computational cell. All solid lattices were similarly oriented with

Cell sizes (scaled by σ^*)	FCC [001]
L_x	12.48
L_y	12.48
L^{fixed} (1 unit cell per end)	1.56
L^{source}	39.00
L^{hs}	21.84
L^{liq}	31.20
L^{cs}	21.84
L^{sink}	39.00
Total length along z axis	156.00

TABLE II. Dimensions of liquid and solid layers in Fig. 2.

the [001] facet plane held parallel to the L/S interfaces. The mass of all liquid and solid particles was set equal to one (reduced units) such that the mass density equalled the number density. Periodic boundary conditions were applied along the \hat{x} and \hat{y} axes.

All particles were made to interact via a truncated and shifted Lennard-Jones potential

$$U_{\text{LJTS}}(r_{ij}) = \begin{cases} U(r_{ij}) - U(r_c) & \text{if } r_{ij} \leq r_c \\ 0 & \text{if } r_{ij} > r_c \end{cases}, \quad (2)$$

where

$$U(r_{ij}) = 4\varepsilon_{ij} \left[\left(\frac{\sigma_{ij}}{r_{ij}} \right)^{12} - \left(\frac{\sigma_{ij}}{r_{ij}} \right)^6 \right]. \quad (3)$$

Subscripts ij denote interacting particle pairs $i/j = L/L$, S/S or L/S , r_{ij} is the pair separation distance, r_c is the interaction cutoff radius, ε_{ij} is the pairwise interaction energy and σ_{ij} is the pairwise distance where $U(r = \sigma_{ij}) = 0$. This form of the Lennard-Jones potential removes the discontinuity introduced by the potential cutoff distance.

The parameter range explored in this study was $(T_{\text{source}}, T_{\text{sink}}) = (1.8, 0.8), (1.6, 1.0)$ and $(1.4, 1.2)$, $\sigma_{LS} = 0.8, 1.0$ or 1.2 and $\varepsilon_{LS} = 0.1, 0.2, \dots, 0.9, 1.0$, the latter spanning non-wetting to completely wetting behavior. The choice of set point temperatures $(T_{\text{source}}, T_{\text{sink}})$ for the Langevin baths ensured that the mid-central region of the liquid layer remained at the average temperature $(T_{\text{source}} + T_{\text{sink}})/2 = 1.3$ and density $\rho_{\text{bulk}} \approx 0.84$ for all runs. This average temperature was chosen to lie far from any critical or triple point [34, 35]. The remaining fixed parameters for all runs were $\sigma_{SS} = 1.0$, $\sigma_{LL} = 1.0$, $\varepsilon_{LL} = 1.0$ and $\varepsilon_{SS} = 10$. Additional information is listed in Tables I and II

Many NEMD studies involving thermal transport in L/S systems have used the harmonic wall-spring model originally introduced to examine the influence of wetting behavior at a fluid/solid interface in equilibrium or under shear. In those studies, the solid portions are constructed by tethering particles to lattice sites using a strong Hookean force [31, 36, 37]. Depending on the pa-

rameter values however, such constructions can dampen or eliminate anharmonic phonon response. In this study, particles in the solid layers were instead made to interact via a strong-binding Lennard-Jones potential [38–40] with $\varepsilon_{SS} = 10$], demonstrated to yield accurate values of mechanical and interfacial properties in FCC metals [41]. Given also that the melting temperature of a Lennard-Jones solid is estimated to be $T_m \simeq \varepsilon_{SS}/2$ [42], the value chosen for ε_{SS} ensured the crystal remained in the solid state throughout the applied temperature range.

The thickness of the solid layers used to enforce thermal control was chosen to exceed that of the unconstrained solid layers in order to avoid spurious reductions in thermal boundary resistance [20]. Studies have shown [20, 43] that when the phonon mean free path in the thermal reservoir region satisfies $\Lambda = c_\ell \times \tau_{\text{damp}} \leq 2L$, where c_ℓ is the speed of longitudinal sound waves, L is the reservoir layer thickness and τ_{damp} is the Langevin damping constant, phonons are dissipated before undergoing reflections from the exterior boundary toward the L/S interface. For an FCC crystal, the value c_ℓ was estimated [42] from the relation $c_\ell = 9.53\sqrt{\varepsilon_{SS}}$. For the parameter values in our study, namely $\tau_{\text{damp}} = 1$ and $L_s = L^{\text{source}} = L^{\text{sink}} = 39$, the inequality $\Lambda = c_\ell \times \tau_{\text{damp}} = 9.53\sqrt{10} \simeq 30 \leq 2L_s = 78$ was therefore well satisfied.

The entire system was first thermally equilibrated using an NVT ensemble implemented with a Nosé–Hoover thermostat [44] set to $T = 1.3$ for a period $t_{eq} = 10^5 \Delta t_{int} = 200$. This thermostat was then replaced by two thermostats [45] acting as the thermal source and sink layers with the motion of each particle constrained by the Langevin equation (reduced units)

$$\frac{d^2\vec{r}_i}{dt^2} = - \sum_{i \neq j} \nabla U_{\text{LJST}} \cdot \vec{r}_{ij} - \frac{1}{\tau_{\text{damp}}} \frac{d\vec{r}_i}{dt} + \vec{F}_{\text{stoch}}, \quad (4)$$

with the damping constant set to $\tau_{\text{damp}} = 500 \Delta t_{int} = 1.0$ and the magnitude of the normally distributed random force \vec{F}_{stoch} set to $[T_s / (\tau_{\text{damp}} \Delta t_{int})]^{1/2}$. As indicated in Fig. 2, T_s was set to T_{source} for the left reservoir and T_{sink} for the right. The entire system was stabilized for an additional period $2 \times 10^5 \Delta t_{int} = 400$ to ensure generation of a steady thermal flux. Once established, measurements of various particle properties in the (unthermostatted) liquid and solid layers were extracted from Newton's equation using second order Verlet integration [33] with a time step $\Delta t_{int} = 0.002$.

The thermal flux across the system was deduced from the relation

$$J_z = \frac{1}{L_x \times L_y} \left\langle \frac{E_{\text{net}}(t)}{t} \right\rangle, \quad (5)$$

where $E_{\text{net}}(t)$ was the system net input energy during the interval t required to maintain the set point temperatures $(T_{\text{source}}, T_{\text{sink}})$. Angular brackets here and elsewhere denote ensemble averaging as described below. It was confirmed that $\langle E_{\text{net}}(t) \rangle$ increased linearly in time, in accord with conditions of constant thermal flux. The mean

and standard deviation of the thermal gradient $|dT/dz|$ in the liquid and solid regions were extracted from linear least squares fits. (The values of the thermal conductivity k in Tables III – V extracted from the Fourier relation $k = J_z/|dT/dz|$ were not used in any part of the analysis but are tabulated there for reference.)

For the parameter values in this study, it was also confirmed that the pressure in the interior of the liquid was far smaller than the values needed to induce measurable reductions in thermal boundary resistance [20]. For example, with $\sigma_{LS} = 1.0$, the virial contribution was $p = 2.72 \pm 0.03$ for $\varepsilon_{LS} = 0.1$ and $p = 2.54 \pm 0.02$ for $\varepsilon_{LS} = 1.0$. Since the interior liquid temperature remained close to $T = 1.3$ by design, the kinetic contribution numbered roughly 1.5.

The layer geometry in Fig. 2 allowed simultaneous measurement of physical quantities in the hotter and colder contact regions, thereby revealing the influence of the local contact layer temperature T_c . The measurements in this study, described in more detail below, included the contact layer temperature and density ρ_c , density depletion layer thickness δ_{LS} (separation distance between the peak density values of the contact layer and first solid layer), thermal gradient in the liquid and solid layers, temperature drop Δ across the L/S interface, thermal slip length L_T , peak value of the in-plane static structure factor of the contact layer S_{\max} , and the frequencies ν_L and ν_S representing the maxima in the phonon density of states spectrum for particles in the contact (L) and first solid (S) layer.

B. Ensemble averaging of stationary quantities

After steady state flux was established, information on particle trajectories was carried out for a total period $t_{\text{total}} = 5 \times 10^6 \Delta t_{\text{int}} = 10^4$. These data strings were divided into ten non-overlapping segments of shorter period 10^3 containing data sampled at intervals $500 \Delta t_{\text{int}} = 1.0$. The sampling interval corresponded to the approximate decay time of the velocity auto-correlation function.

Density and temperature profiles along the \hat{z} axis were obtained by partitioning the liquid and solid layers into non-overlapping bins of volume $L_x \times L_y \times \Delta z_{\text{bin}}$. The bin width $\Delta z_{\text{bin}} = 0.016$ allowed fine resolution of the rapidly decaying oscillations in liquid density near the solid surface. The density in each bin was extracted from the relation $\rho_{\text{bin}} = \langle N_{\text{bin}} \rangle / V_{\text{bin}}$ where N_{bin} is the number of particles in a bin. The distance between neighboring minima of the first oscillation in the liquid density profile was chosen to represent the thickness of the contact layer; the maximum amplitude of that oscillation represents the contact density ρ_c . The distribution of particle speeds within the contact and first solid layer was confirmed to represent Maxwell-Boltzmann statistics. Layer temperatures (based on $\Delta z_{\text{bin}} = 0.785$) were therefore

extracted directly from the equipartition relation

$$T_{\text{bin}} = \left\langle \frac{1}{3 N_{\text{bin}}} \sum_i^{N_{\text{bin}}} \mathbf{v}_i^2 \right\rangle. \quad (6)$$

The temperature drop at the L/S interface was obtained by linear extrapolation of the temperature profile within the interior of the liquid and solid layers. The temperature difference between the two was evaluated at the midpoint of the distance separating the peak densities of the contact and first solid layer. This separation distance is known as the density depletion layer thickness δ_{LS} . The ensemble average of the thermal slip length was then extracted from the relation

$$L_T = \left\langle \frac{\Delta T}{|dT/dz|_{liq}} \right\rangle. \quad (7)$$

Long range translational order within the contact (c) layer was quantified by the 2D static in-plane structure factor [46]

$$S_c^{\parallel}(\vec{k}) = \left\langle \frac{1}{N_c^2} \sum_{p=1}^{N_c} \sum_{q=1}^{N_c} \exp[i\mathbf{k} \cdot (\mathbf{r}_p - \mathbf{r}_q)] \right\rangle, \quad (8)$$

normalized to $0 \leq S_c^{\parallel}(\mathbf{k}) \leq 1$. The superscript \parallel denotes planar values based on the Cartesian coordinates $\mathbf{r} = (x, y)$ and wave numbers $\mathbf{k} = (k_x, k_y)$ representing all particles N_c in the layer. The maximum of Eq. (8), denoted by S_{\max}^{\parallel} , allows coincided with the smallest reciprocal lattice vector of the adjacent solid lattice.

C. Ensemble averaging of time-varying quantities

Measurements of the velocity autocorrelation function extended over the interval $t_{\text{total}} = 1.5 \times 10^6 \Delta t_{\text{int}} = 3 \times 10^3$, which was divided into three equal non-overlapping time blocks initialized at $t_o^B = 0, 10^3$ and 2×10^3 . Velocities in each block were sampled at intervals $10 \Delta t_{\text{int}} = 0.02$, generating a sequence of autocorrelation values over the interval $t_f - t_o$, where $t_o = t_o^B + (0, 10, 20, \dots, 475, 000) \times 0.02$. Since particles in the first solid layer always remained within the layer, the final time could be set to a constant value $t_f = 50$. A different strategy was required for particles in the contact layer since those could exit and enter that layer during the measurement interval. The autocorrelation data was therefore restricted to a subset of particles $N_L(t_o, t_f) \geq 10$ which remained within that layer during the interval $t_f - t_o$. In all cases, this measurement interval exceeded the velocity autocorrelation decay time by at least an order of magnitude.

The phonon density of states per particle $\mathcal{D}(\nu)$ describing the spectrum of normal mode vibrations of particles in the contact and first solid layer was computed from

[47, 48]

$$\mathcal{D}(\nu) = \left\langle \frac{4}{N_L T_L} \int_0^{t_f} \sum_{j=1}^{N_L} \mathbf{v}_j(t_o + t) \cdot \mathbf{v}_j(t_o) \cos(2\pi i \nu t) dt \right\rangle_{t_o}^B, \quad (9)$$

where $\mathbf{v} = (v_x, v_y, v_z)$ and T_L represents the appropriate contact layer temperature. Equation (9) is normalized in accordance with the equipartition theorem requiring $\int_0^\infty \mathcal{D}(\nu) d\nu = 3$. Since different initial times t_o resulted in different final times t_f , the smallest value t_f within each block was used to estimate the mean value for that block; the smallest value t_f over all three blocks was then used to compute the final block (B) average for $\mathcal{D}(\nu)$. The notation $\langle \cdot \rangle_{t_o}^B$ signifies the ensemble average over initial times t_o followed by a three-block average.

III. RESULTS

Shown in Fig. 3(c) is the increase in thermal flux J_z for larger values $T_{\text{source}} - T_{\text{sink}}$ or ε_{LS} and smaller values σ_{LS} . For fixed values $(T_{\text{source}}, T_{\text{sink}})$ and ε_{LS} , the highest thermal flux is achieved with the smallest value σ_{LS} , but this influence on J_z weakens considerably with increasing ε_{LS} . The measured temperature jumps ΔT at the hotter

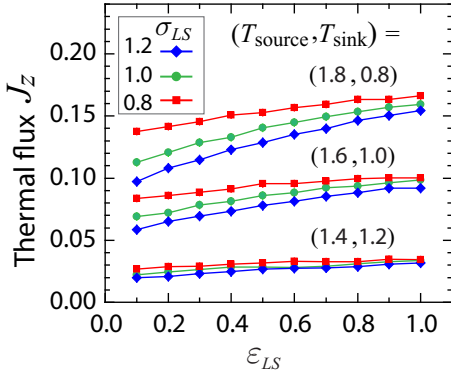


FIG. 3. Measurements of the thermal flux J_z for parameter values $(T_{\text{source}}, T_{\text{sink}})$, ε_{LS} and σ_{LS} .

(H) and colder (C) side of the liquid layer are plotted in Fig. 4. Smaller values ΔT correspond to smaller values of $T_{\text{source}} - T_{\text{sink}}$ or σ_{LS} and larger values ε_{LS} . For fixed values $(T_{\text{source}}, T_{\text{sink}})$ and ε_{LS} , the smallest temperature jump ΔT correlates with the smallest value σ_{LS} .

While both these trends are anticipated, certain parameter values lead to unexpected behavior. For example, it is commonly believed that more frequent collisions within the L/S interface induced by higher temperature will generate a smaller temperature drop ΔT for fixed values $(T_{\text{source}}, T_{\text{sink}})$, ε_{LS} and σ_{LS} . However, closer inspection of the values ΔT in Tables VI - VIII reveals that such reasoning is not always valid. Similar reasoning based exclusively on the kinetic energy of particles has also led to another common misconception that a higher contact density ρ_c leads to a smaller temperature drop

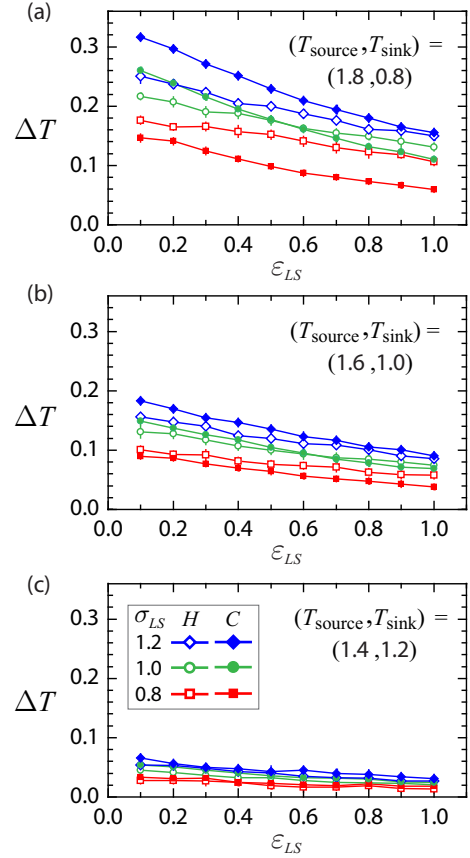


FIG. 4. Dependence of the temperature jump ΔT on given parameter values $(T_{\text{source}}, T_{\text{sink}})$, ε_{LS} and σ_{LS} simultaneously extracted from the hotter (H) and colder (C) side of the liquid layer.

ΔT [49, 50]. However, simulations using larger parameter sets [25] have demonstrated this is not necessarily the case, as evident as well from the values in Tables VI - VIII. The reason, of course, is that the correlation between the thermal slip length L_T and any one parameter or variable fail to capture cooperative effects resulting from the interplay between system parameters. Insights into the conditions generating enhanced thermal transfer and smaller values of L_T require examination of the structural characteristics and frequency response of L/S particle coupling in the contact region.

Shown in Fig. 5(a) - (c) is the reduction in thermal slip length with increasing long range translational order in the contact layer as quantified by the peak value S_{\max}^{\parallel} . Larger values of S_{\max}^{\parallel} are incurred by larger values ε_{LS} , smaller values σ_{LS} and colder interface temperatures. Further inspection of the entries in Tables VI - VIII reveals that of the 180 systems examined, there were six cases for which $S_{\max}^{\parallel} > 0.8$; these correspond to those data points in Fig. 5(a) and (b) exhibiting saturation of S_{\max}^{\parallel} as $\varepsilon_{LS} \rightarrow 1.0$. This behavior is likely representative of quasi-solidification and/or epitaxial formation of the contact layer at the lowest temperatures under highly

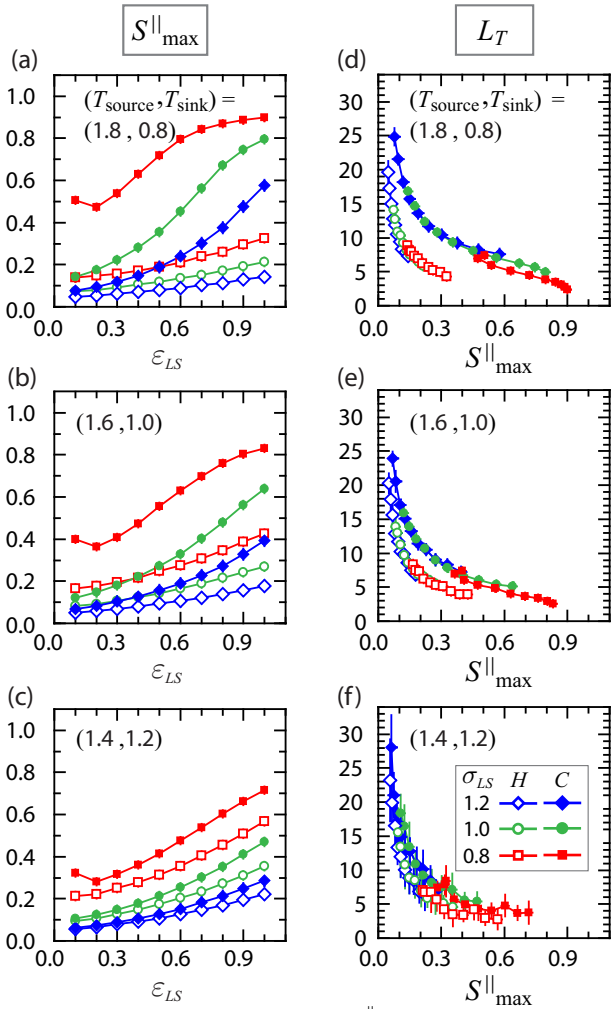


FIG. 5. (a)-(c) Dependence of S_{\max}^{\parallel} on parameter values $(T_{\text{source}}, T_{\text{sink}})$, ε_{LS} and σ_{LS} from simultaneous at the hotter (H) and colder (C) side of the confined liquid layer. (d)-(f) Reduction in L_T with increasing values S_{\max}^{\parallel} . Boxed legend in (f) applies to all six panels shown.

wetting conditions. The data in Fig. 5(a)-(c) for colder contact layers with $\sigma_{LS} = 0.8$ also reveal a sharp transition from solid-like to liquid-like behavior for highly non-wetting substrates with $\varepsilon_{LS} \approx 0.2$. Shown in Fig. 5(d)-(f) is the systematic reduction in L_T with increasing value S_{\max}^{\parallel} . The overall behavior appears to scale with the temperature difference $T_{\text{source}} - T_{\text{sink}}$, which in turn suggests a possible rescaling of the data based on the contact layer temperature T_c .

A nonlinear fit to the proposed relation

$$L_T T_c^2 = a S_{\max}^{-\alpha} . \quad (10)$$

was therefore carried out using orthogonal distance regression incorporating standard deviations in the measured values of L_T , T_c and S_{\max}^{\parallel} . This fit yielded $\alpha = 0.83 \pm 0.02$ and $a = 3.79 \pm 0.14$ where the \pm values denote 95% confidence levels. Reducing the exponent of T_c from 2 to 1.5 resulted in the values $\alpha = 0.74 \pm 0.02$ and $a \simeq 3.94 \pm 0.16$, but the residual sum of squares increased

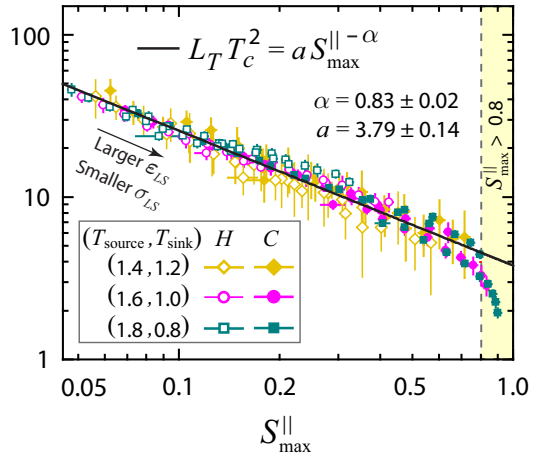


FIG. 6. Collapse of thermal slip length data in the spatial domain with best fit to Eq. (10) (solid line). Excluded from the fit are the six points with $S_{\max} > 0.8$ indicative of a solid-like contact layer.

by 20%. Expanding the regression analysis to three floating variables generated a slight decrease in α from 0.83 ± 0.02 to 0.80 ± 0.03 and a decrease in the exponent for T_c from 2 to 1.83 ± 0.10 . While these current values suggest a general relation of the form $L_T \sim T_c^{-2} S_{\max}^{4/5}$, additional studies on different systems will be required to finalize the values of the exponents and coefficient. Nonetheless, the observed collapse of the data in Fig. 6 is evidence of the strong influence on the thermal slip length of long range translational order in the contact layer further modulated by the local layer temperature.

This result motivated additional analysis of the thermal slip length probing the frequency coupling in the L/S contact zone. The metric for such coupling was chosen to be the ratio of peak frequencies ν_S / ν_L obtained from the phonon spectrum for the density of states of the first solid and contact layer, respectively. An example of such spectra $\mathcal{D}(\nu)$ at the colder side of the liquid layer is shown in Fig. 7(a). In general, the spectrum for the contact layer showed a stronger dependence on ε_{LS} than the first solid layer, as expected. For fixed values $T_{\text{source}} - T_{\text{sink}}$ and σ_{LS} , the magnitude of $\mathcal{D}(\nu = 0)$ was found to undergo a significant decrease as ε_{LS} was increased from 0.1 to 1.0; colder temperatures T_c caused a similar effect. Correspondingly, there occurred a noticeable shift toward higher frequencies in the value ν_L and to a lesser extent in the value ν_S .

It is well known that for a classical isotropic fluid in thermal equilibrium at temperature T consisting of identical particles of mass m , the diffusion constant D is given [47] by $D = (k_B T / 12 m) \mathcal{D}(\nu = 0) =$. The decrease in $\mathcal{D}(\nu = 0)$ with increasing ε_{LS} or colder temperatures T_c therefore signifies a reduction in the mobility of particles due to tighter binding with the vibrational motion of the first solid layer. The results in Fig. 7(b)-(d) confirm that stronger coupling in the L/S contact zone - whether by larger values ε_{LS} , smaller values σ_{LS} or lower temper-

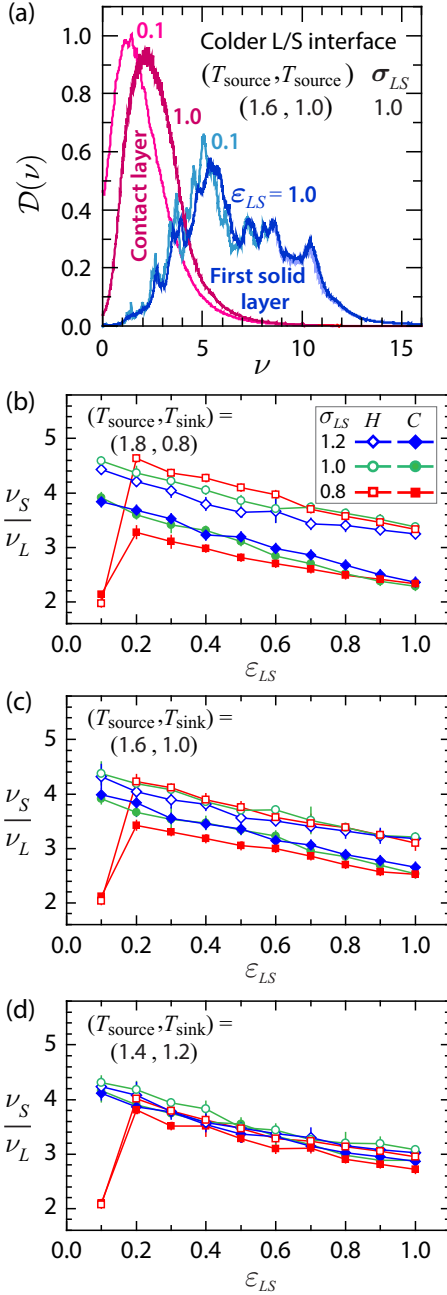


FIG. 7. (a) Example of frequency spectrum per particle $D(\nu)$ for the contact and first solid layer extracted from the colder L/S interface for parameter values $(T_{\text{source}}, T_{\text{sink}}) = (1.6, 1.0)$, $\sigma_{LS} = 1.0$ and $\varepsilon_{LS} = 0.1$ and 1.0. (b) - (d) Dependence of the frequency ratio ν_S/ν_L on $(T_{\text{source}}, T_{\text{sink}})$, ε_{LS} and σ_{LS} simultaneously extracted from the hotter (H) and colder (C) side of the liquid layer.

atures T_c - leads to better frequency matching as characterized by a smaller ratio ν_S/ν_L . We note in passing that the six data points in Fig. 7(b)-(d) corresponding to runs with $\varepsilon_{LS} = 0.1$ and $\sigma_{LS} = 0.8$ generated the smallest ratios $\nu_S/\nu_L \approx 2$ likely indicative of a phase transition leading to quasi-solidification and/or epitaxial formation of the contact layer induced by the combina-

tion of a highly non-wetting substrate but smaller L/S repulsive distance.

Shown in Fig. 8 is a collapse of the data excluding the unusual phase with $\varepsilon_{LS} = 0.1$ and $\sigma_{LS} = 0.8$. The solid line represents a nonlinear fit to the relation

$$L_T T_c^{3/2} / \sigma_{LS}^2 = b \left(\nu_S / \nu_L \right)^\beta. \quad (11)$$

using orthogonal distance regression incorporating standard deviations in the measured values of L_T , T_c and ν_S/ν_L . The resulting fit yielded values for the exponent $\beta = 2.93 \pm 0.11$ and coefficient $b = 0.35 \pm 0.05$, where the \pm values denote 95% confidence levels. Expanding the regression analysis to three floating variables resulted in little change to the exponent of σ_{LS} exponent, a small increase from 1.5 to 1.61 ± 0.13 in the exponent of T_c and an even smaller increase from 2.93 ± 0.11 to 2.98 ± 0.14 in the exponent β . Regression trials based on third order polynomials led to substantially worse fits. Our regression analysis therefore suggests the relation $L_T \sim \sigma_{LS}^2 T_c^{-3/2} (\nu_S / \nu_L)^3$.

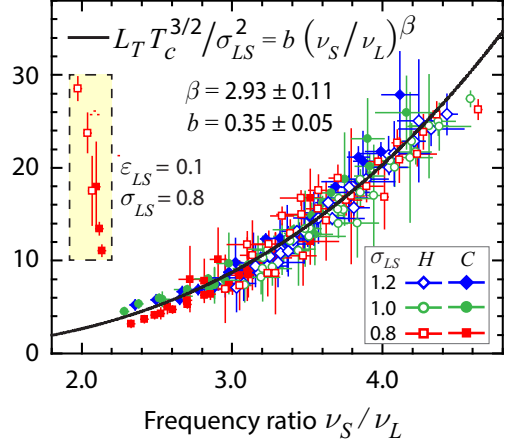


FIG. 8. Collapse of thermal slip length data in the frequency domain with best fit to Eq. (11) (solid line). Excluded from the fit are the six points with $\nu_S/\nu_L \approx 2$ indicative of a solid-like contact layer.

IV. CONCLUSION

The NEMD study described in this work was specifically designed to elicit the dependence of the thermal slip length on collective properties of the L/S contact zone as modulated by local interactions and local temperature. The dimensions and facet planes of the FCC lattice comprising the solid layers were held constant throughout so as to isolate the influence of the solid surface potential on the contact layer. The power law equations extracted from the data highlight the important role of in-plane long range translational order and peak vibrational frequency coupling within the L/S contact zone. The data spanning 180 systems show excellent collapse onto the

power law relation

$$L_T \sim T_c^{-2} S_{\max}^{\parallel 4/5}, \quad (12)$$

for behavior in the spatial domain and

$$L_T \sim \sigma_{LS}^2 T_c^{-3/2} (\nu_S/\nu_L)^3, \quad (13)$$

in the frequency domain.

While more studies are obviously needed to establish the generality of these equations, we anticipate similar relations to emerge from studies of different Lennard-Jones systems given the principle of corresponding states governing this interaction potential [41, 51]. Based on these current results however, it seems that future focus on *surface localized phonons* is likely to yield valuable insights into other features of the L/S contact zone responsible for smaller thermal slip lengths. Such insights can in-

centivize new generation “de novo” designs of integrated chips capable of ultra high power density and excellent energy efficiency.

V. DATA AVAILABILITY STATEMENT

All data in support of the findings are provided in Tables III - XI of the Appendix.

ACKNOWLEDGMENTS

The authors gratefully acknowledge funding from a 2019 NASA Space Technology Research Fellowship (HK) as well as the assistance of Dr. Peter Thompson, who administers the LIS2T computing cluster used in this work.

-
- [1] R. van Erp, R. Soleimanzadeh, L. Nela, G. Kampitsis, and E. Matioli, Co-designing electronics with microfluidics for more sustainable cooling, *Nature* **585**, 211 (2020).
 - [2] G. Rak, IBM demos transistor built for liquid nitrogen cooling, <https://spectrum.ieee.org/nanosheet-transistor> (2023).
 - [3] S. Rangarajan, S. N. Schiffres, and B. Sammakia, A review of recent developments in “on-chip” embedded cooling technologies for heterogeneous integrated applications, *Engineering* **26**, 185 (2023).
 - [4] R. Saligram, A. Raychowdhury, and S. Datta, The future is frozen: cryogenic CMOS for high-performance computing, *Chip* **3**, 100082 (2024).
 - [5] I. M. Khalatnikov, Teploobmen mezhdu tverdym telom i Geliem-ii, *Zh. Eksp. Teor. Fiz.* **22**, 687 (1952).
 - [6] G. L. Pollack, Kapitza resistance, *Rev. Mod. Phys.* **41**, 48 (1969).
 - [7] E. T. Swartz and R. O. Pohl, Thermal boundary resistance, *Rev. Mod. Phys.* **61**, 605 (1989).
 - [8] P. A. Thompson and S. M. Troian, A general boundary condition for liquid flow at solid surfaces, *Nature* **389**, 360 (1997).
 - [9] J.-L. Barrat and L. Bocquet, Influence of wetting properties on hydrodynamic boundary conditions at a fluid/solid interface, *Faraday Discuss.* **112**, 119 (1999).
 - [10] N. V. Priezjev and S. M. Troian, Molecular origin and dynamic behavior of slip in sheared polymer films, *Phys. Rev. Lett.* **92**, 018302 (2004).
 - [11] N. V. Priezjev, A. A. Darhuber, and S. M. Troian, Slip behavior in liquid films on surfaces of patterned wettability: Comparison between continuum and molecular dynamics, *Phys. Rev. E* **71**, 041608 (2005).
 - [12] N. V. Priezjev and S. M. Troian, Influence of periodic wall roughness on the slip behaviour at liquid/solid interfaces: molecular-scale simulations versus continuum predictions, *J. Fluid Mech.* **554**, 24 (2006).
 - [13] S. Matsumoto, Molecular dynamics simulation of a liquid droplet on a solid surface, *J. Jap. Soc. Tribologists* **42**, 93 (1997).
 - [14] S. Maruyama, T. Kurashige, S. Matsumoto, Y. Yamaguchi, and T. Kimura, Liquid droplet in contact with a solid surface, *Micro. Thermophys. Eng.* **2**, 49 (1998).
 - [15] T. Ohara and D. Suzuki, Intermolecular energy transfer at a solid–liquid interface, *Micro. Thermophys. Eng.* **4**, 189 (2000).
 - [16] J.-L. Barrat and F. Chiaruttini, Kapitza resistance at the liquid–solid interface, *Mol. Phys.* **101**, 1605 (2003).
 - [17] L. Xue, P. Kebelinski, S. R. Phillpot, S. U.-S. Choi, and J. A. Eastman, Two regimes of thermal resistance at a liquid–solid interface, *J. Chem. Phys.* **118**, 337 (2003).
 - [18] Y. Wang and P. Kebelinski, Role of wetting and nanoscale roughness on thermal conductance at liquid–solid interface, *Appl. Phys. Lett.* **99**, 073112 (2011).
 - [19] S. Murad and I. K. Puri, Thermal transport across nanoscale solid–fluid interfaces, *Appl. Phys. Lett.* **92**, 133105 (2008).
 - [20] H. Han, S. Mérabia, and F. Müller-Plathe, Thermal transport at solid–liquid interfaces: High pressure facilitates heat flow through nonlocal liquid structuring, *J. Phys. Chem. Lett.* **8**, 1946 (2017).
 - [21] G. Balasubramanian, S. Banerjee, and I. K. Puri, Unsteady nanoscale thermal transport across a solid–fluid interface, *J. Appl. Phys.* **104**, 064306 (2008).
 - [22] A. K. M. M. Morshed, T. Paul, and J. A. Khan, Atomistic simulation of temperature dependent thermal transport across nanoconfined liquid, *Physica E* **47**, 246 (2013).
 - [23] T. Ohara and D. Torii, Molecular dynamics study of thermal phenomena in an ultrathin liquid film sheared between solid surfaces: The influence of the crystal plane on energy and momentum transfer at solid-liquid interfaces, *J. Chem. Phys.* **122**, 214717 (2005).
 - [24] D. Torii, T. Ohara, and K. Ishida, Molecular-scale mechanism of thermal resistance at the solid–liquid interfaces: Influence of interaction parameters between solid and liquid molecules, *J. Heat Transfer* **132**, 012402 (2010).
 - [25] H. Kaifu, S. M. Troian, and A. I. Baskin, How caged motion in the contact layer enhances thermal tunneling across a liquid/solid interface, *Phys. Rev. Research* **6**, 033123 (2024).
 - [26] B. H. Kim, A. Beskok, and T. Cagin, Molecular dynamics simulations of thermal resistance at the liquid-solid interface, *J. Chem. Phys.* **129**, 174701 (2008).
 - [27] B. Ramos-Alvarado, S. Kumar, and G. P. Peterson, Solid–liquid thermal transport and its relationship with wettability and the interfacial liquid structure, *J. Phys.*

- Chem. Lett. **7**, 3497 (2016).
- [28] C. U. Gonzalez-Valle, S. Kumar, and B. Ramos-Alvarado, Thermal transport across SiC-water interfaces, ACS Appl. Mater. Interfaces **10**, 29179 (2018).
- [29] S. Li, Y. Chen, J. Zhao, C. Wang, and N. Wei, Atomic structure causing an obvious difference in thermal conductance at the Pd–H₂O interface: A molecular dynamics simulation, Nanoscale **12**, 17870 (2020).
- [30] S. Plimpton, Fast parallel algorithms for short-range molecular dynamics, J. Comput. Phys. **117**, 1 (1995).
- [31] A. P. Thompson, H. M. Aktulga, R. Berger, D. S. Bolintineanu, W. M. Brown, P. S. Crozier, P. J. in 't Velde, A. Kohlmeyer, S. G. Moore, T. D. Nguyen, R. Shan, M. J. Stevens, J. Tranchida, C. Trott, and S. J. Plimpton, LAMMPS – A flexible simulation tool for particle-based materials modeling at the atomic, meso, and continuum scales, Comp. Phys. Comm. **271**, 108171 (2022).
- [32] A. Michels, H. Wijker, and H. Wijker, Isotherms of argon between 0°C and 150°C and pressures up to 2900 atmospheres, Physica **XV**, 627 (1949).
- [33] L. Verlet, Computer “experiments” on classical fluids. i. Thermodynamical properties of Lennard-Jones molecules, Phys. Rev. **159**, 98 (1967).
- [34] B. L. Holian and D. J. Evans, Shear viscosities away from the melting line: A comparison of equilibrium and nonequilibrium molecular dynamics, J. Chem. Phys. **78**, 5147 (1983).
- [35] M. Thol, G. Rutkai, A. Köster, R. Lustig, R. Span, and J. Vrabec, Equation of state for the Lennard-Jones fluid, J. Phys. Chem. Ref. Data **45**, 023101 (2016).
- [36] M. Cieplak, J. Koplik, and J. R. Banavar, Boundary conditions at a fluid–solid interface, Phys. Rev. Lett. **86**, 803 (2001).
- [37] J. H. Sikkenk, J. O. Indekeu, J. M. J. van Leeuwen, E. O. Vossnaek, and A. F. Bakker, Simulation of wetting and drying at solid-fluid interfaces on the Delft molecular dynamics processor, J. Stat. Phys. **52**, 23 (1988).
- [38] A. Giri and P. E. Hopkins, Spectral analysis of thermal boundary conductance across solid/classical liquid interfaces: A molecular dynamics study, Appl. Phys. Lett. **105**, 033106 (2014).
- [39] K. Sääskilahti, J. Oksanen, J. Tulkki, and S. Volz, Spectral mapping of heat transfer mechanisms at liquid-solid interfaces, Phys. Rev. E **93**, 052141 (2016).
- [40] M. R. Hasan, T. Q. Vo, and B. Kim, Manipulating thermal resistance at the solid–fluid interface through monolayer deposition, RSC Adv. **9**, 4948 (2019).
- [41] K. Kanhaiya, S. Kim, W. Im, and H. Heinz, Accurate simulation of surfaces and interfaces of ten FCC metals and steel using Lennard–Jones potentials, NPJ Comput. Mater. **7**, 17 (2021).
- [42] R. J. Stevens, L. V. Zhigilei, and P. M. Norris, Effects of temperature and disorder on thermal boundary conductance at solid–solid interfaces: Nonequilibrium molecular dynamics simulations, Int. J. Mech. Sci. **50**, 3977 (2007).
- [43] Z. Liang and P. Kebinski, Finite-size effects on molecular dynamics interfacial thermal-resistance predictions, Phys. Rev. B **90**, 075411 (2014).
- [44] W. G. Hoover, Canonical dynamics: Equilibrium phase-space distributions, Phys. Rev. A **31**, 1695 (1985).
- [45] T. Schneider and E. Stoll, Molecular-dynamics study of a three-dimensional one-component model for distortive phase transitions, Phys. Rev. B **17**, 1302 (1978).
- [46] In many studies of the L/S interface, the liquid structure factor is often computed from the relation $|\sum_p^{N_c} \exp(-ik \cdot r_p)|^2$, a simplification strictly valid for particles on sites of a Bravais lattice.
- [47] P. H. Berens, D. H. J. Mackay, G. M. White, and K. R. Wilson, Thermodynamics and quantum corrections from molecular dynamics for liquid water, J. Chem. Phys. **79**, 2375 (1983).
- [48] S. T. Lin, M. Blanco, and W. A. Goddard, The two-phase model for calculating thermodynamic properties of liquids from molecular dynamics: Validation for the phase diagram of Lennard-Jones fluids, J. Chem. Phys. **119**, 11792 (2003).
- [49] S. Murad and I. K. Puri, Molecular simulation of thermal transport across hydrophilic interfaces, Chem. Phys. Lett. **467**, 110 (2008).
- [50] A. Pham, M. Barisik, and B. Kim, Pressure dependence of Kapitza resistance at gold/water and silicon/water interfaces, J. Chem. Phys. **139**, 244702 (2013).
- [51] E. Helfand and S. A. Rice, Principle of corresponding states for transport properties, J. Chem. Phys. **32**, 1642 (1960).

APPENDIX

TABLE III. Measured values of the mean and standard deviation (in parenthesis) for the thermal flux J_z and thermal gradient magnitude $|dT/dz|$ in the interior liquid and solid layers for parameter values $(T_{\text{source}}, T_{\text{sink}}) = (1.8, 0.8)$, $\sigma_{LS} = 0.8, 1.0$ and 1.2 and $\varepsilon_{LS} = 0.1, 0.2, \dots, 0.9, 1.0$. All quantities are in reduced units defined in Table I. Column headings specify multiplicative factor for numerical entries.

σ_{LS}	ε_{LS}	$J_z [10^{-2}]$	Liquid layer		Hotter solid layer		Colder solid layer	
			$ dT/dz [10^{-2}]$	k	$ dT/dz [10^{-4}]$	$k [10^2]$	$ dT/dz [10^{-4}]$	$k [10^2]$
0.8	0.1	13.74(0.05)	1.99(0.03)	6.93(0.10)	9.29(1.98)	1.52(0.37)	4.85(0.69)	2.86(0.44)
0.8	0.2	14.15(0.06)	2.04(0.03)	6.94(0.11)	9.89(1.89)	1.52(0.35)	4.95(0.73)	2.88(0.44)
0.8	0.3	14.55(0.08)	2.09(0.03)	6.95(0.10)	8.11(1.53)	1.81(0.32)	4.55(0.73)	3.18(0.44)
0.8	0.4	15.06(0.09)	2.15(0.03)	6.99(0.10)	9.34(1.58)	1.69(0.29)	4.58(0.93)	3.41(0.77)
0.8	0.5	15.26(0.08)	2.20(0.03)	6.92(0.11)	10.42(1.30)	1.51(0.19)	4.27(1.16)	3.56(0.87)
0.8	0.6	15.67(0.05)	2.28(0.02)	6.89(0.07)	10.08(2.06)	1.60(0.40)	5.19(1.01)	2.93(0.39)
0.8	0.7	15.94(0.04)	2.32(0.02)	6.89(0.07)	11.45(1.99)	1.47(0.29)	5.46(0.81)	3.03(0.39)
0.8	0.8	16.34(0.09)	2.37(0.03)	6.90(0.09)	10.86(1.85)	1.55(0.28)	5.36(1.09)	2.99(0.45)
0.8	0.9	16.33(0.06)	2.40(0.02)	6.80(0.07)	11.05(2.54)	1.54(0.32)	5.02(0.94)	3.48(0.85)
0.8	1.0	16.62(0.03)	2.46(0.02)	6.75(0.06)	9.98(1.18)	1.67(0.19)	5.58(1.08)	3.12(0.72)
1.0	0.1	11.26(0.05)	1.54(0.01)	7.30(0.07)	7.57(2.19)	1.57(0.47)	4.01(0.40)	2.87(0.30)
1.0	0.2	12.06(0.03)	1.63(0.04)	7.42(0.17)	8.14(1.18)	1.53(0.25)	4.42(0.94)	2.92(0.53)
1.0	0.3	12.87(0.04)	1.75(0.03)	7.38(0.12)	8.71(1.85)	1.55(0.32)	4.76(0.83)	2.79(0.70)
1.0	0.4	13.29(0.08)	1.82(0.02)	7.32(0.11)	9.14(2.15)	1.48(0.36)	4.59(0.92)	3.08(0.66)
1.0	0.5	14.06(0.05)	1.91(0.03)	7.37(0.11)	8.15(1.07)	1.77(0.25)	5.31(1.07)	2.74(0.63)
1.0	0.6	14.49(0.04)	2.00(0.02)	7.27(0.06)	9.61(2.25)	1.60(0.51)	5.38(0.96)	2.80(0.58)
1.0	0.7	14.94(0.05)	2.06(0.03)	7.26(0.09)	10.76(2.95)	1.39(0.34)	5.23(0.97)	2.99(0.66)
1.0	0.8	15.35(0.05)	2.12(0.02)	7.25(0.05)	9.76(1.34)	1.61(0.24)	5.61(0.68)	2.79(0.42)
1.0	0.9	15.71(0.05)	2.17(0.02)	7.23(0.05)	10.94(0.90)	1.44(0.12)	5.46(0.67)	2.92(0.40)
1.0	1.0	15.94(0.10)	2.25(0.03)	7.09(0.10)	9.68(2.07)	1.77(0.45)	5.32(1.11)	3.07(0.74)
1.2	0.1	9.72(0.10)	1.28(0.05)	7.60(0.24)	6.23(1.51)	1.69(0.67)	3.64(0.93)	2.88(1.00)
1.2	0.2	10.79(0.06)	1.37(0.02)	7.83(0.14)	6.58(1.54)	1.75(0.56)	4.20(0.72)	2.67(0.45)
1.2	0.3	11.48(0.04)	1.49(0.02)	7.70(0.10)	7.24(2.15)	1.72(0.55)	3.90(0.82)	3.10(0.82)
1.2	0.4	12.28(0.01)	1.60(0.02)	7.64(0.08)	8.64(0.87)	1.44(0.16)	3.96(1.02)	3.39(0.78)
1.2	0.5	12.86(0.04)	1.69(0.02)	7.64(0.11)	8.23(1.92)	1.62(0.44)	4.68(0.68)	2.85(0.48)
1.2	0.6	13.50(0.06)	1.79(0.02)	7.55(0.10)	8.41(1.74)	1.71(0.41)	4.62(1.43)	3.30(0.88)
1.2	0.7	13.99(0.09)	1.87(0.03)	7.49(0.16)	9.15(2.17)	1.66(0.45)	5.05(0.46)	2.79(0.27)
1.2	0.8	14.66(0.04)	1.94(0.03)	7.52(0.14)	10.52(1.64)	1.42(0.29)	5.32(0.72)	2.86(0.44)
1.2	0.9	15.05(0.06)	2.01(0.02)	7.49(0.06)	9.48(1.23)	1.64(0.20)	5.27(0.97)	3.03(0.52)
1.2	1.0	15.44(0.04)	2.06(0.03)	7.48(0.11)	9.33(1.92)	1.78(0.29)	5.01(0.95)	3.06(0.52)

TABLE IV. Measured values of the mean and standard deviation (in parenthesis) for the thermal flux J_z and thermal gradient magnitude $|dT/dz|$ in the interior liquid and solid layers for parameter values $(T_{\text{source}}, T_{\text{sink}}) = (1.6, 1.0)$, $\sigma_{LS} = 0.8, 1.0$ and 1.2 and $\varepsilon_{LS} = 0.1, 0.2, \dots, 0.9, 1.0$. All quantities are in reduced units defined in Table I. Column headings specify multiplicative factor for numerical entries.

σ_{LS}	ε_{LS}	$J_z [10^{-2}]$	Liquid layer		Hotter solid layer		Colder solid layer	
			$ dT/dz [10^{-2}]$	k	$ dT/dz [10^{-4}]$	$k [10^2]$	$ dT/dz [10^{-4}]$	$k [10^2]$
0.8	0.1	8.35(0.05)	1.21(0.03)	6.92(0.14)	4.74(1.61)	1.86(0.66)	3.44(0.85)	2.52(0.62)
0.8	0.2	8.59(0.03)	1.24(0.02)	6.91(0.11)	4.52(1.12)	2.13(0.80)	3.14(0.86)	3.09(1.43)
0.8	0.3	8.84(0.03)	1.27(0.03)	7.01(0.17)	5.56(1.28)	1.58(0.32)	3.89(1.65)	2.29(0.86)
0.8	0.4	9.12(0.02)	1.32(0.02)	6.94(0.12)	5.66(1.66)	1.79(0.60)	3.81(1.04)	2.55(0.85)
0.8	0.5	9.55(0.02)	1.35(0.03)	7.12(0.12)	6.03(1.78)	1.73(0.49)	4.05(1.26)	2.50(1.15)
0.8	0.6	9.54(0.06)	1.38(0.02)	6.89(0.13)	5.44(1.41)	1.93(0.65)	3.62(0.88)	2.83(0.68)
0.8	0.7	9.76(0.03)	1.40(0.03)	6.97(0.16)	5.11(2.42)	2.48(1.96)	4.11(1.10)	2.48(0.75)
0.8	0.8	9.96(0.03)	1.44(0.02)	6.95(0.10)	6.26(1.92)	1.68(0.48)	4.27(0.77)	2.44(0.50)
0.8	0.9	10.02(0.08)	1.47(0.02)	6.81(0.11)	5.51(1.37)	1.84(0.41)	3.84(1.30)	3.04(1.06)
0.8	1.0	10.02(0.04)	1.48(0.02)	6.77(0.11)	5.95(1.94)	1.98(0.72)	4.53(1.38)	2.67(1.53)
1.0	0.1	6.91(0.08)	0.94(0.03)	7.38(0.24)	4.54(1.58)	1.89(1.00)	2.87(0.97)	2.49(0.94)
1.0	0.2	7.19(0.03)	0.99(0.02)	7.29(0.16)	4.68(1.81)	1.95(1.05)	3.20(0.84)	2.44(0.53)
1.0	0.3	7.84(0.03)	1.05(0.04)	7.46(0.30)	4.41(2.15)	2.14(1.15)	3.58(1.10)	2.27(0.71)
1.0	0.4	8.14(0.02)	1.10(0.03)	7.39(0.18)	4.92(1.97)	1.83(0.73)	3.48(1.66)	2.56(1.33)
1.0	0.5	8.60(0.03)	1.17(0.03)	7.35(0.19)	4.31(1.15)	2.14(0.65)	3.42(0.67)	2.61(0.54)
1.0	0.6	8.82(0.05)	1.22(0.03)	7.27(0.19)	4.87(2.04)	2.38(1.47)	3.27(1.34)	2.77(1.10)
1.0	0.7	9.21(0.07)	1.27(0.03)	7.28(0.25)	5.22(1.69)	2.06(0.76)	3.60(1.33)	2.74(1.18)
1.0	0.8	9.34(0.07)	1.29(0.03)	7.24(0.15)	5.21(1.59)	1.92(0.94)	3.32(1.08)	2.84(0.85)
1.0	0.9	9.62(0.05)	1.33(0.02)	7.25(0.13)	5.64(1.25)	1.75(0.36)	3.95(0.92)	2.51(0.78)
1.0	1.0	9.84(0.05)	1.35(0.03)	7.26(0.15)	6.11(1.64)	1.66(0.43)	3.85(1.34)	3.01(1.62)
1.2	0.1	5.84(0.04)	0.77(0.03)	7.60(0.29)	4.07(1.56)	1.90(1.29)	2.32(0.80)	2.65(0.94)
1.2	0.2	6.53(0.05)	0.83(0.04)	7.88(0.35)	4.06(1.70)	2.14(1.49)	3.06(0.89)	2.19(0.61)
1.2	0.3	6.94(0.09)	0.90(0.03)	7.69(0.25)	3.89(1.16)	2.01(0.98)	2.45(0.92)	3.23(1.09)
1.2	0.4	7.33(0.02)	0.97(0.03)	7.56(0.23)	4.15(2.09)	2.19(1.24)	3.61(0.90)	2.13(0.65)
1.2	0.5	7.79(0.02)	1.02(0.02)	7.67(0.15)	4.56(1.34)	1.86(0.84)	3.60(1.16)	2.49(1.15)
1.2	0.6	8.15(0.03)	1.08(0.02)	7.53(0.14)	5.45(1.94)	2.03(1.72)	3.25(1.65)	3.35(1.48)
1.2	0.7	8.53(0.03)	1.11(0.02)	7.69(0.17)	5.46(1.82)	1.74(0.60)	3.31(0.99)	2.93(0.86)
1.2	0.8	8.81(0.10)	1.17(0.03)	7.53(0.23)	5.30(1.91)	1.87(0.75)	3.59(1.27)	3.43(3.27)
1.2	0.9	9.18(0.05)	1.21(0.02)	7.61(0.15)	6.13(1.17)	1.57(0.37)	3.23(0.61)	2.74(0.34)
1.2	1.0	9.18(0.04)	1.26(0.02)	7.31(0.11)	5.82(1.39)	1.66(0.38)	3.70(0.74)	2.61(0.60)

TABLE V. Measured values of the mean and standard deviation (in parenthesis) for the thermal flux J_z and thermal gradient magnitude $|dT/dz|$ in the interior liquid and solid layers for parameter values $(T_{\text{source}}, T_{\text{sink}}) = (1.4, 1.2)$, $\sigma_{LS} = 0.8, 1.0$ and 1.2 and $\varepsilon_{LS} = 0.1, 0.2, \dots, 0.9, 1.0$. All quantities are in reduced units defined in Table I. Column headings specify multiplicative factor for numerical entries.

σ_{LS}	ε_{LS}	$J_z [10^{-2}]$	Liquid layer		Hotter solid layer		Colder solid layer	
			$ dT/dz [10^{-2}]$	k	$ dT/dz [10^{-4}]$	$k [10^2]$	$ dT/dz [10^{-4}]$	$k [10^2]$
0.8	0.1	2.67(0.04)	0.41(0.03)	6.64(0.55)	2.24(1.07)	1.55(0.80)	1.08(0.91)	7.54(8.04)
0.8	0.2	2.89(0.06)	0.42(0.02)	6.93(0.36)	1.46(0.86)	2.49(1.70)	0.99(1.01)	8.58(10.23)
0.8	0.3	2.92(0.04)	0.41(0.04)	7.23(0.59)	1.92(1.50)	3.20(3.41)	1.55(1.30)	4.01(4.66)
0.8	0.4	3.08(0.04)	0.44(0.02)	7.02(0.41)	2.13(1.29)	2.31(2.18)	1.77(1.09)	15.50(40.90)
0.8	0.5	3.18(0.04)	0.47(0.02)	6.84(0.31)	2.26(1.03)	1.86(1.32)	1.18(0.69)	4.68(4.26)
0.8	0.6	3.32(0.03)	0.48(0.02)	6.88(0.29)	2.11(1.10)	3.52(4.71)	1.30(0.92)	14.13(30.41)
0.8	0.7	3.28(0.03)	0.49(0.02)	6.73(0.22)	1.36(1.60)	6.64(6.66)	0.99(0.99)	9.77(11.11)
0.8	0.8	3.26(0.06)	0.47(0.03)	7.03(0.50)	1.92(1.44)	3.26(4.03)	1.68(1.25)	5.31(7.72)
0.8	0.9	3.47(0.03)	0.49(0.02)	7.08(0.27)	1.54(0.77)	3.35(2.41)	1.59(1.33)	18.50(40.33)
0.8	1.0	3.42(0.07)	0.49(0.02)	6.93(0.34)	2.06(1.19)	2.47(1.53)	1.85(1.10)	5.23(7.45)
1.0	0.1	2.23(0.02)	0.30(0.03)	7.73(0.72)	1.76(1.13)	3.86(6.72)	1.89(1.18)	2.53(3.85)
1.0	0.2	2.45(0.03)	0.31(0.04)	7.88(0.95)	2.33(1.79)	9.41(22.71)	0.83(0.52)	4.52(2.78)
1.0	0.3	2.66(0.04)	0.35(0.04)	7.87(0.74)	1.56(1.15)	8.15(14.80)	1.84(1.34)	2.11(1.37)
1.0	0.4	2.84(0.07)	0.37(0.03)	7.63(0.49)	1.97(1.63)	6.16(10.34)	1.10(0.81)	5.83(6.36)
1.0	0.5	2.84(0.04)	0.39(0.03)	7.34(0.61)	1.72(1.23)	3.63(4.71)	1.82(1.38)	7.43(14.99)
1.0	0.6	2.82(0.04)	0.41(0.04)	6.93(0.59)	2.30(1.18)	1.63(0.71)	1.98(1.21)	2.69(3.40)
1.0	0.7	2.93(0.03)	0.43(0.03)	6.92(0.39)	1.90(1.17)	4.21(5.75)	1.57(1.33)	10.83(18.10)
1.0	0.8	3.10(0.04)	0.43(0.04)	7.25(0.65)	1.88(0.93)	2.56(1.98)	1.72(1.00)	6.66(14.53)
1.0	0.9	3.28(0.02)	0.46(0.02)	7.23(0.31)	2.13(1.37)	3.60(4.59)	1.04(0.99)	5.39(3.76)
1.0	1.0	3.38(0.02)	0.46(0.02)	7.46(0.26)	1.71(0.99)	3.28(2.79)	1.86(1.18)	4.94(8.89)
1.2	0.1	1.99(0.02)	0.24(0.03)	8.63(0.92)	1.22(1.30)	5.52(4.64)	1.51(1.36)	9.00(17.51)
1.2	0.2	2.10(0.07)	0.27(0.02)	7.83(0.80)	0.70(0.48)	5.19(4.74)	1.37(0.94)	1.94(1.16)
1.2	0.3	2.32(0.05)	0.30(0.02)	7.91(0.71)	1.71(1.37)	2.77(3.32)	1.50(0.64)	4.67(9.31)
1.2	0.4	2.48(0.01)	0.32(0.03)	7.73(0.67)	1.34(0.69)	2.71(2.42)	1.70(1.18)	2.50(2.39)
1.2	0.5	2.66(0.06)	0.34(0.04)	7.97(0.70)	1.28(0.59)	2.32(1.08)	1.89(1.27)	9.55(21.16)
1.2	0.6	2.75(0.07)	0.35(0.02)	7.89(0.56)	1.62(1.22)	9.61(22.48)	1.14(0.60)	3.43(2.15)
1.2	0.7	2.79(0.02)	0.37(0.03)	7.58(0.61)	2.12(1.46)	9.80(24.50)	1.65(0.82)	2.40(2.24)
1.2	0.8	2.87(0.07)	0.38(0.03)	7.59(0.63)	1.60(1.31)	14.86(36.81)	1.67(1.44)	4.31(5.32)
1.2	0.9	3.07(0.04)	0.41(0.03)	7.66(0.63)	2.15(1.14)	7.33(17.54)	1.67(0.95)	3.36(3.06)
1.2	1.0	3.17(0.05)	0.43(0.02)	7.46(0.46)	1.52(1.52)	21.41(54.65)	1.14(0.76)	8.50(13.81)

TABLE VI. Mean and standard deviation (in parenthesis) for the contact layer density ρ_c , density depletion layer thickness δ_{LS} , maximum value of the in-plane static structure factor of the contact layer S_{max}^{\parallel} , contact layer temperature T_c , interface temperature drop ΔT and thermal slip length L_T measured at the hotter and colder L/S interface for parameter values $(T_{source}, T_{sink}) = (1.8, 0.8)$, $\sigma_{LS} = 0.8, 1.0$ and 1.2 and $\varepsilon_{LS} = 0.1, 0.2, \dots, 0.9, 1.0$. All quantities are in reduced units defined in Table I.

Hotter L/S interface						Colder L/S interface							
σ_{LS}	ε_{LS}	ρ_c	δ_{LS}	S_{max}^{\parallel}	T_c	ΔT	L_T	ρ_c	δ_{LS}	S_{max}^{\parallel}	T_c	ΔT	L_T
0.8	0.1	0.922(0.018)	0.646(0.008)	0.139(0.001)	1.618(0.007)	0.176(0.007)	8.871(0.386)	0.995(0.019)	0.465(0.010)	0.507(0.008)	0.973(0.005)	0.147(0.007)	7.377(0.398)
0.8	0.2	1.021(0.009)	0.657(0.009)	0.147(0.002)	1.627(0.006)	0.165(0.005)	8.097(0.317)	1.263(0.015)	0.487(0.007)	0.473(0.003)	0.970(0.002)	0.141(0.006)	6.908(0.378)
0.8	0.3	1.075(0.029)	0.665(0.008)	0.156(0.002)	1.629(0.008)	0.166(0.007)	7.926(0.419)	1.474(0.031)	0.468(0.000)	0.539(0.004)	0.955(0.005)	0.124(0.006)	5.933(0.355)
0.8	0.4	1.116(0.013)	0.666(0.008)	0.171(0.001)	1.634(0.007)	0.157(0.010)	7.313(0.556)	1.774(0.031)	0.452(0.000)	0.631(0.006)	0.943(0.003)	0.111(0.004)	5.142(0.225)
0.8	0.5	1.153(0.011)	0.655(0.000)	0.190(0.002)	1.641(0.006)	0.152(0.008)	6.901(0.419)	2.113(0.028)	0.452(0.000)	0.720(0.004)	0.931(0.003)	0.098(0.003)	4.469(0.159)
0.8	0.6	1.195(0.018)	0.643(0.007)	0.209(0.002)	1.657(0.004)	0.141(0.008)	6.194(0.393)	2.492(0.039)	0.437(0.000)	0.796(0.003)	0.920(0.004)	0.087(0.005)	3.816(0.238)
0.8	0.7	1.217(0.014)	0.638(0.005)	0.238(0.003)	1.664(0.004)	0.130(0.009)	5.628(0.418)	2.845(0.048)	0.437(0.000)	0.842(0.003)	0.915(0.002)	0.080(0.004)	3.467(0.176)
0.8	0.8	1.245(0.032)	0.629(0.008)	0.261(0.002)	1.673(0.004)	0.123(0.010)	5.193(0.494)	3.134(0.044)	0.435(0.005)	0.870(0.002)	0.907(0.003)	0.073(0.004)	3.073(0.155)
0.8	0.9	1.293(0.026)	0.622(0.005)	0.295(0.002)	1.680(0.006)	0.118(0.005)	4.920(0.222)	3.383(0.049)	0.431(0.008)	0.887(0.001)	0.901(0.003)	0.067(0.005)	2.773(0.216)
0.8	1.0	1.340(0.019)	0.608(0.000)	0.325(0.003)	1.691(0.004)	0.106(0.006)	4.310(0.269)	3.589(0.027)	0.431(0.008)	0.899(0.001)	0.895(0.003)	0.060(0.003)	2.420(0.153)
1.0	0.1	1.292(0.036)	0.847(0.008)	0.073(0.001)	1.562(0.004)	0.217(0.005)	14.052(0.425)	1.641(0.029)	0.811(0.000)	0.142(0.002)	1.088(0.004)	0.260(0.006)	16.845(0.382)
1.0	0.2	1.381(0.022)	0.883(0.008)	0.081(0.001)	1.570(0.009)	0.207(0.008)	12.722(0.765)	1.822(0.009)	0.842(0.000)	0.174(0.002)	1.068(0.003)	0.239(0.006)	14.655(0.643)
1.0	0.3	1.456(0.021)	0.891(0.005)	0.092(0.001)	1.582(0.007)	0.190(0.009)	10.903(0.616)	1.994(0.026)	0.842(0.000)	0.222(0.003)	1.053(0.005)	0.216(0.005)	12.359(0.406)
1.0	0.4	1.536(0.025)	0.891(0.005)	0.106(0.001)	1.590(0.009)	0.188(0.009)	10.339(0.561)	2.160(0.026)	0.838(0.008)	0.281(0.003)	1.031(0.004)	0.195(0.005)	10.743(0.356)
1.0	0.5	1.596(0.024)	0.892(0.007)	0.119(0.001)	1.603(0.006)	0.176(0.008)	9.226(0.525)	2.386(0.037)	0.827(0.000)	0.356(0.006)	1.015(0.005)	0.178(0.007)	9.308(0.459)
1.0	0.6	1.646(0.034)	0.903(0.005)	0.135(0.001)	1.614(0.004)	0.163(0.004)	8.145(0.243)	2.630(0.041)	0.827(0.000)	0.453(0.005)	0.998(0.004)	0.161(0.004)	8.053(0.257)
1.0	0.7	1.716(0.035)	0.900(0.008)	0.152(0.002)	1.625(0.008)	0.154(0.007)	7.484(0.428)	3.016(0.051)	0.811(0.000)	0.561(0.005)	0.984(0.003)	0.146(0.005)	7.061(0.323)
1.0	0.8	1.770(0.017)	0.889(0.000)	0.171(0.001)	1.635(0.006)	0.149(0.005)	7.037(0.306)	3.390(0.030)	0.811(0.000)	0.670(0.004)	0.972(0.003)	0.132(0.003)	6.220(0.157)
1.0	0.9	1.862(0.029)	0.889(0.000)	0.192(0.001)	1.637(0.008)	0.140(0.009)	6.443(0.452)	3.759(0.052)	0.805(0.008)	0.746(0.004)	0.963(0.005)	0.123(0.005)	5.641(0.185)
1.0	1.0	1.933(0.023)	0.889(0.000)	0.214(0.002)	1.651(0.007)	0.131(0.007)	5.836(0.356)	4.079(0.053)	0.797(0.005)	0.795(0.002)	0.951(0.002)	0.110(0.004)	4.894(0.225)
1.2	0.1	1.439(0.027)	1.045(0.000)	0.048(0.001)	1.527(0.011)	0.250(0.012)	19.648(1.642)	1.797(0.030)	1.022(0.008)	0.076(0.001)	1.145(0.004)	0.316(0.006)	24.821(1.281)
1.2	0.2	1.574(0.019)	1.078(0.005)	0.054(0.001)	1.537(0.006)	0.237(0.007)	17.257(0.792)	1.991(0.022)	1.062(0.005)	0.094(0.002)	1.126(0.005)	0.297(0.004)	21.613(0.574)
1.2	0.3	1.672(0.024)	1.100(0.008)	0.062(0.001)	1.549(0.007)	0.224(0.007)	14.973(0.574)	2.170(0.030)	1.076(0.000)	0.118(0.002)	1.102(0.004)	0.271(0.005)	18.148(0.413)
1.2	0.4	1.754(0.035)	1.108(0.000)	0.070(0.001)	1.565(0.007)	0.205(0.008)	12.768(0.625)	2.339(0.040)	1.086(0.008)	0.149(0.002)	1.087(0.003)	0.252(0.005)	15.680(0.409)
1.2	0.5	1.851(0.017)	1.123(0.000)	0.080(0.001)	1.573(0.008)	0.200(0.006)	11.857(0.512)	2.544(0.031)	1.092(0.000)	0.189(0.003)	1.065(0.003)	0.229(0.004)	13.582(0.350)
1.2	0.6	1.913(0.030)	1.123(0.000)	0.090(0.001)	1.585(0.005)	0.187(0.007)	10.485(0.459)	2.777(0.035)	1.092(0.000)	0.238(0.003)	1.050(0.004)	0.210(0.006)	11.726(0.404)
1.2	0.7	2.021(0.033)	1.125(0.005)	0.104(0.001)	1.592(0.004)	0.176(0.005)	9.431(0.365)	2.983(0.035)	1.090(0.005)	0.302(0.005)	1.035(0.005)	0.194(0.007)	10.426(0.510)
1.2	0.8	2.078(0.024)	1.126(0.007)	0.114(0.002)	1.610(0.007)	0.161(0.008)	8.291(0.506)	3.215(0.033)	1.086(0.008)	0.375(0.007)	1.025(0.004)	0.180(0.005)	9.249(0.388)
1.2	0.9	2.172(0.026)	1.123(0.000)	0.131(0.002)	1.613(0.007)	0.159(0.004)	7.904(0.248)	3.534(0.034)	1.076(0.000)	0.475(0.006)	1.008(0.004)	0.165(0.006)	8.210(0.367)
1.2	1.0	2.259(0.031)	1.123(0.000)	0.142(0.001)	1.624(0.007)	0.150(0.007)	7.269(0.438)	3.824(0.047)	1.076(0.000)	0.577(0.008)	0.999(0.004)	0.156(0.005)	7.547(0.365)

TABLE VII. Mean and standard deviation (in parenthesis) for the contact layer density ρ_c , density depletion layer thickness δ_{LS} , maximum value of the in-plane static structure factor of the contact layer S_{max}^{\parallel} , contact layer temperature T_c , interface temperature drop ΔT and thermal slip length L_T measured at the hotter and colder L/S interface for parameter values $(T_{\text{source}}, T_{\text{sink}}) = (1.6, 0.1)$, $\sigma_{LS} = 0.8, 1.0$ and 1.2 and $\varepsilon_{LS} = 0.1, 0.2, \dots, 0.9, 1.0$. All quantities are in reduced units defined in Table I.

Hotter L/S interface							Colder L/S interface						
σ_{LS}	ε_{LS}	ρ_c	δ_{LS}	S_{max}^{\parallel}	T_c	ΔT	L_T	ρ_c	δ_{LS}	S_{max}^{\parallel}	T_c	ΔT	L_T
0.8	0.1	0.946(0.029)	0.624(0.007)	0.166(0.002)	1.493(0.003)	0.100(0.007)	8.330(0.739)	0.993(0.020)	0.512(0.010)	0.400(0.007)	1.101(0.004)	0.090(0.004)	7.440(0.354)
0.8	0.2	1.066(0.025)	0.629(0.008)	0.178(0.002)	1.500(0.005)	0.093(0.004)	7.472(0.430)	1.198(0.030)	0.546(0.000)	0.365(0.002)	1.102(0.003)	0.086(0.003)	6.928(0.317)
0.8	0.3	1.129(0.017)	0.640(0.000)	0.195(0.002)	1.500(0.005)	0.092(0.009)	7.268(0.833)	1.300(0.024)	0.537(0.008)	0.409(0.002)	1.095(0.003)	0.077(0.004)	6.075(0.427)
0.8	0.4	1.168(0.018)	0.632(0.008)	0.216(0.002)	1.507(0.007)	0.082(0.006)	6.221(0.558)	1.444(0.029)	0.513(0.005)	0.474(0.004)	1.089(0.004)	0.070(0.005)	5.332(0.393)
0.8	0.5	1.224(0.015)	0.627(0.007)	0.247(0.003)	1.514(0.007)	0.076(0.006)	5.679(0.556)	1.615(0.022)	0.493(0.008)	0.555(0.003)	1.082(0.005)	0.065(0.006)	4.800(0.476)
0.8	0.6	1.258(0.014)	0.616(0.008)	0.276(0.002)	1.518(0.007)	0.074(0.004)	5.334(0.373)	1.844(0.027)	0.484(0.000)	0.629(0.005)	1.075(0.004)	0.056(0.005)	4.049(0.379)
0.8	0.7	1.312(0.017)	0.607(0.005)	0.308(0.002)	1.520(0.006)	0.072(0.008)	5.125(0.659)	2.083(0.025)	0.468(0.000)	0.699(0.003)	1.071(0.003)	0.052(0.004)	3.685(0.330)
0.8	0.8	1.349(0.016)	0.593(0.000)	0.345(0.004)	1.531(0.006)	0.063(0.006)	4.380(0.479)	2.339(0.031)	0.468(0.000)	0.759(0.003)	1.066(0.004)	0.048(0.005)	3.337(0.393)
0.8	0.9	1.415(0.032)	0.576(0.005)	0.386(0.004)	1.534(0.004)	0.058(0.006)	3.974(0.463)	2.581(0.037)	0.456(0.007)	0.803(0.002)	1.060(0.004)	0.043(0.006)	2.939(0.407)
0.8	1.0	1.479(0.018)	0.560(0.005)	0.425(0.002)	1.537(0.005)	0.058(0.006)	3.932(0.473)	2.792(0.042)	0.443(0.008)	0.832(0.001)	1.057(0.003)	0.038(0.005)	2.546(0.332)
1.0	0.1	1.350(0.027)	0.841(0.005)	0.082(0.002)	1.454(0.008)	0.131(0.010)	13.930(1.421)	1.552(0.025)	0.813(0.005)	0.120(0.001)	1.171(0.005)	0.149(0.007)	15.911(1.003)
1.0	0.2	1.462(0.021)	0.872(0.005)	0.093(0.001)	1.458(0.007)	0.128(0.008)	12.975(1.070)	1.710(0.033)	0.842(0.000)	0.147(0.002)	1.157(0.004)	0.137(0.006)	13.913(0.698)
1.0	0.3	1.550(0.022)	0.889(0.000)	0.107(0.001)	1.471(0.008)	0.118(0.008)	11.241(1.139)	1.872(0.020)	0.849(0.008)	0.180(0.003)	1.148(0.007)	0.126(0.007)	12.070(1.085)
1.0	0.4	1.623(0.020)	0.889(0.000)	0.124(0.001)	1.474(0.007)	0.107(0.007)	9.701(0.797)	1.995(0.023)	0.858(0.000)	0.220(0.002)	1.139(0.003)	0.118(0.005)	10.652(0.653)
1.0	0.5	1.716(0.020)	0.886(0.007)	0.143(0.002)	1.483(0.007)	0.100(0.007)	8.588(0.805)	2.139(0.037)	0.852(0.008)	0.273(0.003)	1.127(0.007)	0.105(0.008)	8.992(0.855)
1.0	0.6	1.794(0.015)	0.881(0.008)	0.165(0.003)	1.492(0.005)	0.093(0.008)	7.688(0.823)	2.303(0.050)	0.842(0.000)	0.329(0.006)	1.118(0.004)	0.095(0.006)	7.819(0.580)
1.0	0.7	1.869(0.035)	0.878(0.008)	0.189(0.003)	1.498(0.006)	0.087(0.008)	6.893(0.780)	2.505(0.023)	0.839(0.007)	0.402(0.003)	1.110(0.004)	0.085(0.006)	6.718(0.566)
1.0	0.8	1.954(0.027)	0.875(0.005)	0.215(0.002)	1.498(0.007)	0.085(0.005)	6.596(0.536)	2.721(0.037)	0.833(0.008)	0.479(0.004)	1.102(0.004)	0.078(0.005)	6.067(0.515)
1.0	0.9	2.025(0.030)	0.875(0.005)	0.242(0.002)	1.504(0.006)	0.080(0.008)	6.017(0.666)	2.989(0.033)	0.816(0.008)	0.562(0.005)	1.095(0.005)	0.071(0.007)	5.361(0.568)
1.0	1.0	2.112(0.025)	0.874(0.000)	0.270(0.002)	1.515(0.008)	0.075(0.005)	5.536(0.476)	3.279(0.031)	0.811(0.000)	0.640(0.007)	1.089(0.007)	0.069(0.008)	5.122(0.681)
1.2	0.1	1.514(0.017)	1.045(0.000)	0.051(0.001)	1.431(0.006)	0.156(0.007)	20.334(1.460)	1.701(0.020)	1.039(0.008)	0.069(0.001)	1.197(0.003)	0.183(0.003)	23.918(1.048)
1.2	0.2	1.637(0.029)	1.076(0.000)	0.059(0.001)	1.436(0.008)	0.148(0.008)	17.882(1.652)	1.897(0.035)	1.073(0.007)	0.084(0.001)	1.188(0.007)	0.170(0.006)	20.539(1.536)
1.2	0.3	1.752(0.034)	1.094(0.005)	0.069(0.001)	1.443(0.006)	0.141(0.009)	15.586(1.435)	2.077(0.021)	1.081(0.008)	0.103(0.002)	1.176(0.005)	0.154(0.003)	17.080(0.793)
1.2	0.4	1.856(0.024)	1.108(0.000)	0.080(0.001)	1.457(0.005)	0.125(0.004)	12.851(0.638)	2.208(0.016)	1.092(0.000)	0.126(0.002)	1.167(0.005)	0.147(0.006)	15.092(0.962)
1.2	0.5	1.968(0.024)	1.109(0.005)	0.093(0.001)	1.465(0.008)	0.120(0.006)	11.744(0.748)	2.390(0.045)	1.092(0.000)	0.157(0.003)	1.155(0.005)	0.135(0.002)	13.289(0.417)
1.2	0.6	2.031(0.027)	1.119(0.008)	0.105(0.001)	1.471(0.009)	0.111(0.009)	10.240(0.916)	2.541(0.026)	1.092(0.000)	0.188(0.003)	1.148(0.007)	0.123(0.008)	11.407(0.862)
1.2	0.7	2.149(0.039)	1.123(0.000)	0.121(0.002)	1.473(0.007)	0.109(0.004)	9.831(0.520)	2.717(0.040)	1.092(0.000)	0.227(0.003)	1.136(0.004)	0.117(0.006)	10.540(0.727)
1.2	0.8	2.251(0.019)	1.123(0.000)	0.139(0.001)	1.481(0.007)	0.100(0.007)	8.606(0.805)	2.863(0.032)	1.092(0.000)	0.273(0.003)	1.129(0.004)	0.105(0.006)	9.010(0.705)
1.2	0.9	2.346(0.022)	1.123(0.000)	0.158(0.001)	1.487(0.006)	0.091(0.006)	7.497(0.548)	3.046(0.020)	1.092(0.000)	0.329(0.004)	1.124(0.004)	0.100(0.006)	8.324(0.626)
1.2	1.0	2.439(0.035)	1.115(0.008)	0.177(0.002)	1.495(0.005)	0.086(0.005)	6.835(0.422)	3.300(0.054)	1.092(0.000)	0.394(0.004)	1.113(0.005)	0.090(0.005)	7.183(0.459)

TABLE VIII. Mean and standard deviation (in parenthesis) for the contact layer density ρ_c , density depletion layer thickness δ_{LS} , maximum value of the in-plane static structure factor of the contact layer S_{max}^{\parallel} , contact layer temperature T_c , interface temperature drop ΔT and thermal slip length L_T measured at the hotter and colder L/S interface for parameter values $(T_{\text{source}}, T_{\text{sink}}) = (1.4, 1.2)$, $\sigma_{LS} = 0.8, 1.0$ and 1.2 and $\varepsilon_{LS} = 0.1, 0.2, \dots, 0.9, 1.0$. All quantities are in reduced units defined in Table I.

Hotter L/S interface						Colder L/S interface							
σ_{LS}	ε_{LS}	ρ_c	δ_{LS}	S_{max}^{\parallel}	T_c	ΔT	L_T	ρ_c	δ_{LS}	$S_{\parallel max}$	T_c	ΔT	L_T
0.8	0.1	0.973(0.019)	0.599(0.008)	0.213(0.003)	1.366(0.007)	0.028(0.004)	7.023(1.477)	0.949(0.018)	0.619(0.104)	0.324(0.009)	1.235(0.004)	0.033(0.007)	8.382(2.217)
0.8	0.2	1.106(0.019)	0.615(0.008)	0.223(0.002)	1.371(0.006)	0.028(0.005)	6.722(1.352)	1.145(0.017)	0.580(0.007)	0.280(0.003)	1.234(0.003)	0.031(0.004)	7.388(0.910)
0.8	0.3	1.186(0.017)	0.610(0.005)	0.252(0.002)	1.369(0.007)	0.027(0.008)	6.769(2.898)	1.247(0.016)	0.582(0.008)	0.318(0.002)	1.234(0.004)	0.032(0.003)	7.819(1.441)
0.8	0.4	1.248(0.016)	0.608(0.000)	0.278(0.002)	1.369(0.005)	0.025(0.006)	5.712(1.689)	1.317(0.023)	0.566(0.008)	0.362(0.003)	1.231(0.004)	0.025(0.004)	5.657(1.132)
0.8	0.5	1.282(0.023)	0.599(0.008)	0.315(0.002)	1.374(0.004)	0.019(0.005)	4.189(1.259)	1.390(0.023)	0.544(0.005)	0.414(0.004)	1.228(0.005)	0.023(0.005)	4.939(1.131)
0.8	0.6	1.353(0.029)	0.580(0.007)	0.354(0.002)	1.376(0.003)	0.016(0.008)	3.433(1.727)	1.526(0.024)	0.521(0.008)	0.477(0.004)	1.226(0.003)	0.021(0.007)	4.283(1.590)
0.8	0.7	1.418(0.014)	0.563(0.009)	0.404(0.003)	1.379(0.005)	0.017(0.004)	3.413(0.953)	1.660(0.021)	0.499(0.000)	0.539(0.004)	1.224(0.006)	0.019(0.005)	4.009(1.124)
0.8	0.8	1.511(0.026)	0.540(0.008)	0.454(0.004)	1.378(0.003)	0.019(0.006)	4.186(1.465)	1.822(0.030)	0.495(0.008)	0.603(0.002)	1.227(0.005)	0.022(0.006)	4.781(1.573)
0.8	0.9	1.614(0.024)	0.516(0.005)	0.508(0.004)	1.380(0.006)	0.014(0.005)	2.900(1.025)	2.018(0.055)	0.484(0.000)	0.661(0.004)	1.224(0.005)	0.018(0.005)	3.695(1.087)
0.8	1.0	1.771(0.015)	0.505(0.008)	0.567(0.003)	1.382(0.005)	0.013(0.007)	2.745(1.429)	2.196(0.033)	0.480(0.007)	0.715(0.002)	1.225(0.005)	0.018(0.008)	3.780(1.657)
1.0	0.1	1.414(0.033)	0.839(0.007)	0.094(0.001)	1.352(0.004)	0.045(0.006)	15.579(3.516)	1.472(0.016)	0.822(0.008)	0.105(0.002)	1.260(0.004)	0.054(0.004)	18.331(2.761)
1.0	0.2	1.531(0.036)	0.864(0.008)	0.107(0.002)	1.352(0.011)	0.041(0.010)	13.439(4.419)	1.628(0.026)	0.847(0.008)	0.125(0.002)	1.253(0.004)	0.051(0.006)	16.480(3.067)
1.0	0.3	1.638(0.029)	0.874(0.000)	0.126(0.001)	1.358(0.006)	0.036(0.008)	10.760(3.410)	1.742(0.025)	0.858(0.000)	0.148(0.002)	1.251(0.005)	0.046(0.008)	13.431(3.536)
1.0	0.4	1.736(0.029)	0.875(0.005)	0.149(0.002)	1.357(0.006)	0.033(0.006)	8.869(2.284)	1.874(0.031)	0.858(0.000)	0.178(0.002)	1.246(0.004)	0.040(0.004)	10.904(1.702)
1.0	0.5	1.839(0.030)	0.880(0.008)	0.175(0.002)	1.360(0.005)	0.032(0.008)	8.467(2.537)	1.966(0.039)	0.858(0.000)	0.214(0.002)	1.242(0.007)	0.036(0.007)	9.263(2.347)
1.0	0.6	1.925(0.039)	0.877(0.007)	0.203(0.002)	1.364(0.007)	0.028(0.008)	6.953(2.313)	2.111(0.016)	0.858(0.000)	0.255(0.003)	1.242(0.005)	0.033(0.006)	8.112(1.942)
1.0	0.7	2.027(0.033)	0.867(0.008)	0.234(0.002)	1.369(0.005)	0.025(0.004)	5.818(1.220)	2.215(0.041)	0.858(0.000)	0.302(0.004)	1.239(0.004)	0.032(0.006)	7.474(1.686)
1.0	0.8	2.132(0.020)	0.863(0.008)	0.272(0.003)	1.370(0.004)	0.024(0.007)	5.695(2.158)	2.341(0.028)	0.852(0.008)	0.352(0.003)	1.233(0.006)	0.030(0.008)	7.095(2.375)
1.0	0.9	2.238(0.021)	0.858(0.000)	0.310(0.002)	1.373(0.004)	0.023(0.005)	5.094(1.096)	2.529(0.040)	0.842(0.000)	0.412(0.004)	1.229(0.003)	0.025(0.005)	5.542(1.161)
1.0	1.0	2.344(0.021)	0.855(0.007)	0.354(0.003)	1.373(0.006)	0.021(0.005)	4.574(1.118)	2.687(0.025)	0.841(0.005)	0.471(0.003)	1.230(0.005)	0.025(0.006)	5.394(1.397)
1.2	0.1	1.575(0.027)	1.041(0.008)	0.057(0.001)	1.342(0.006)	0.054(0.009)	23.224(6.058)	1.637(0.026)	1.044(0.005)	0.062(0.001)	1.268(0.005)	0.065(0.006)	28.098(4.700)
1.2	0.2	1.710(0.025)	1.076(0.000)	0.065(0.001)	1.343(0.005)	0.053(0.005)	19.911(3.191)	1.800(0.019)	1.076(0.000)	0.073(0.001)	1.261(0.008)	0.056(0.005)	21.058(3.257)
1.2	0.3	1.845(0.023)	1.092(0.000)	0.078(0.001)	1.347(0.006)	0.048(0.007)	16.513(3.461)	1.958(0.023)	1.090(0.005)	0.090(0.001)	1.258(0.004)	0.050(0.005)	17.104(2.421)
1.2	0.4	1.947(0.019)	1.100(0.008)	0.092(0.002)	1.351(0.006)	0.042(0.005)	13.374(2.473)	2.087(0.022)	1.108(0.000)	0.107(0.001)	1.256(0.006)	0.047(0.005)	14.870(2.902)
1.2	0.5	2.079(0.035)	1.108(0.000)	0.108(0.002)	1.355(0.009)	0.041(0.009)	12.002(3.082)	2.224(0.028)	1.103(0.008)	0.128(0.002)	1.251(0.006)	0.043(0.009)	12.753(3.622)
1.2	0.6	2.223(0.031)	1.108(0.000)	0.127(0.002)	1.354(0.006)	0.035(0.007)	10.064(2.430)	2.346(0.042)	1.101(0.008)	0.152(0.002)	1.252(0.004)	0.045(0.005)	12.803(1.907)
1.2	0.7	2.312(0.041)	1.109(0.005)	0.147(0.003)	1.360(0.005)	0.033(0.007)	8.908(2.334)	2.514(0.037)	1.098(0.008)	0.183(0.002)	1.247(0.004)	0.040(0.007)	10.875(2.502)
1.2	0.8	2.434(0.027)	1.108(0.000)	0.168(0.002)	1.363(0.006)	0.032(0.006)	8.517(2.008)	2.651(0.045)	1.097(0.008)	0.212(0.003)	1.244(0.005)	0.038(0.008)	10.158(2.714)
1.2	0.9	2.556(0.036)	1.114(0.008)	0.195(0.002)	1.365(0.005)	0.027(0.005)	6.823(1.653)	2.762(0.025)	1.097(0.008)	0.249(0.002)	1.240(0.004)	0.034(0.007)	8.481(2.092)
1.2	1.0	2.669(0.042)	1.111(0.007)	0.222(0.002)	1.365(0.006)	0.027(0.008)	6.427(2.324)	2.924(0.047)	1.094(0.005)	0.286(0.002)	1.237(0.004)	0.031(0.002)	7.228(0.766)

TABLE IX. Mean and standard deviation (in parenthesis) for the peak vibrational frequencies ν_L and ν_S and ratio ν_S/ν_L [extracted from Eq. (9)] for particles in the contact (L) and first solid (S) layer at the hotter and colder L/S interface for parameter values $(T_{\text{source}}, T_{\text{sink}}) = (1.8, 0.8)$, $\sigma_{LS} = 0.8, 1.0$ and 1.2 and $\varepsilon_{LS} = 0.1, 0.2, \dots, 0.8, 1.0$. All quantities are in reduced units defined in Table I.

σ_{LS}	ε_{LS}	Hotter L/S interface			Colder L/S interface		
		ν_L	ν_S	ν_S/ν_L	ν_L	ν_S	ν_S/ν_L
0.8	0.1	2.453(0.021)	4.843(0.006)	1.974(0.015)	2.377(0.006)	5.070(0.000)	2.133(0.005)
0.8	0.2	1.050(0.000)	4.870(0.014)	4.638(0.013)	1.563(0.055)	5.120(0.000)	3.278(0.115)
0.8	0.3	1.123(0.012)	4.900(0.000)	4.362(0.045)	1.660(0.062)	5.147(0.006)	3.103(0.118)
0.8	0.4	1.150(0.017)	4.913(0.006)	4.273(0.066)	1.740(0.017)	5.183(0.006)	2.979(0.026)
0.8	0.5	1.200(0.010)	4.920(0.000)	4.100(0.034)	1.857(0.015)	5.227(0.012)	2.815(0.023)
0.8	0.6	1.243(0.021)	4.937(0.006)	3.971(0.068)	1.947(0.012)	5.260(0.000)	2.702(0.016)
0.8	0.7	1.337(0.021)	4.950(0.010)	3.704(0.060)	2.037(0.012)	5.300(0.000)	2.602(0.015)
0.8	0.8	1.390(0.026)	4.967(0.006)	3.574(0.066)	2.150(0.010)	5.343(0.012)	2.485(0.013)
0.8	0.9	1.443(0.055)	4.987(0.006)	3.458(0.137)	2.230(0.010)	5.387(0.006)	2.416(0.013)
0.8	1.0	1.503(0.031)	5.007(0.012)	3.331(0.076)	2.330(0.010)	5.427(0.006)	2.329(0.008)
1.0	0.1	1.073(0.006)	4.923(0.006)	4.587(0.019)	1.317(0.032)	5.150(0.000)	3.913(0.097)
1.0	0.2	1.133(0.029)	4.950(0.000)	4.370(0.113)	1.437(0.006)	5.173(0.006)	3.601(0.013)
1.0	0.3	1.177(0.031)	4.963(0.006)	4.220(0.104)	1.527(0.060)	5.203(0.006)	3.412(0.137)
1.0	0.4	1.230(0.020)	4.983(0.006)	4.052(0.066)	1.583(0.025)	5.243(0.006)	3.312(0.049)
1.0	0.5	1.300(0.030)	5.007(0.006)	3.853(0.093)	1.700(0.040)	5.283(0.006)	3.109(0.070)
1.0	0.6	1.360(0.090)	5.030(0.010)	3.709(0.239)	1.877(0.064)	5.327(0.012)	2.840(0.088)
1.0	0.7	1.350(0.026)	5.050(0.010)	3.742(0.067)	1.990(0.061)	5.377(0.006)	2.704(0.085)
1.0	0.8	1.403(0.032)	5.083(0.006)	3.624(0.078)	2.160(0.020)	5.430(0.017)	2.514(0.017)
1.0	0.9	1.450(0.026)	5.100(0.017)	3.518(0.053)	2.313(0.023)	5.503(0.006)	2.379(0.025)
1.0	1.0	1.527(0.038)	5.147(0.025)	3.372(0.072)	2.433(0.006)	5.560(0.000)	2.285(0.005)
1.2	0.1	1.120(0.017)	4.960(0.000)	4.429(0.068)	1.347(0.025)	5.170(0.000)	3.840(0.072)
1.2	0.2	1.183(0.021)	4.980(0.000)	4.209(0.075)	1.410(0.017)	5.197(0.012)	3.686(0.042)
1.2	0.3	1.240(0.035)	5.010(0.010)	4.043(0.122)	1.487(0.031)	5.237(0.012)	3.523(0.074)
1.2	0.4	1.330(0.040)	5.047(0.006)	3.797(0.114)	1.633(0.021)	5.267(0.015)	3.225(0.032)
1.2	0.5	1.393(0.032)	5.070(0.010)	3.640(0.082)	1.670(0.010)	5.323(0.012)	3.188(0.014)
1.2	0.6	1.397(0.076)	5.110(0.010)	3.666(0.211)	1.800(0.017)	5.360(0.000)	2.978(0.029)
1.2	0.7	1.500(0.046)	5.143(0.012)	3.431(0.098)	1.897(0.006)	5.427(0.006)	2.861(0.006)
1.2	0.8	1.523(0.045)	5.183(0.012)	3.405(0.107)	2.053(0.025)	5.480(0.010)	2.669(0.031)
1.2	0.9	1.573(0.012)	5.227(0.006)	3.322(0.021)	2.213(0.021)	5.523(0.006)	2.496(0.026)
1.2	1.0	1.627(0.035)	5.283(0.012)	3.249(0.076)	2.363(0.012)	5.567(0.012)	2.355(0.016)

TABLE X. Mean and standard deviation (in parenthesis) for the peak vibrational frequencies ν_L and ν_S and ratio ν_S/ν_L [extracted from Eq. (9)] for particles in the contact (L) and first solid (S) layer at the hotter and colder L/S interface for parameter values $(T_{\text{source}}, T_{\text{sink}}) = (1.6, 1.0)$, $\sigma_{LS} = 0.8, 1.0$ and 1.2 and $\varepsilon_{LS} = 0.1, 0.2, \dots, 0.8, 1.0$. All quantities are in reduced units defined in Table I.

σ_{LS}	ε_{LS}	Hotter L/S interface			Colder L/S interface		
		ν_L	ν_S	ν_S/ν_L	ν_L	ν_S	ν_S/ν_L
0.8	0.1	2.407(0.012)	4.903(0.006)	2.037(0.007)	2.383(0.006)	5.047(0.006)	2.117(0.004)
0.8	0.2	1.170(0.036)	4.947(0.006)	4.230(0.125)	1.483(0.038)	5.080(0.000)	3.426(0.089)
0.8	0.3	1.207(0.006)	4.963(0.006)	4.113(0.018)	1.547(0.025)	5.110(0.010)	3.304(0.057)
0.8	0.4	1.280(0.036)	4.980(0.000)	3.893(0.111)	1.617(0.038)	5.137(0.006)	3.178(0.072)
0.8	0.5	1.330(0.035)	4.997(0.006)	3.759(0.102)	1.697(0.038)	5.170(0.000)	3.048(0.067)
0.8	0.6	1.403(0.029)	5.010(0.000)	3.571(0.074)	1.733(0.031)	5.200(0.000)	3.001(0.053)
0.8	0.7	1.453(0.067)	5.023(0.012)	3.461(0.162)	1.833(0.021)	5.237(0.006)	2.857(0.030)
0.8	0.8	1.490(0.010)	5.047(0.006)	3.387(0.019)	1.957(0.023)	5.283(0.006)	2.700(0.031)
0.8	0.9	1.563(0.049)	5.067(0.015)	3.243(0.100)	2.070(0.017)	5.320(0.000)	2.570(0.022)
0.8	1.0	1.643(0.070)	5.090(0.000)	3.101(0.133)	2.120(0.010)	5.353(0.006)	2.525(0.012)
1.0	0.1	1.137(0.051)	4.970(0.010)	4.379(0.208)	1.307(0.032)	5.113(0.006)	3.915(0.096)
1.0	0.2	1.193(0.025)	5.003(0.006)	4.194(0.089)	1.407(0.023)	5.147(0.006)	3.659(0.057)
1.0	0.3	1.230(0.026)	5.020(0.010)	4.083(0.097)	1.467(0.087)	5.167(0.006)	3.531(0.211)
1.0	0.4	1.310(0.020)	5.047(0.006)	3.853(0.055)	1.500(0.053)	5.200(0.000)	3.469(0.120)
1.0	0.5	1.370(0.000)	5.073(0.006)	3.703(0.004)	1.570(0.040)	5.243(0.006)	3.341(0.085)
1.0	0.6	1.377(0.021)	5.103(0.006)	3.708(0.059)	1.633(0.042)	5.277(0.012)	3.232(0.087)
1.0	0.7	1.463(0.101)	5.127(0.012)	3.514(0.238)	1.803(0.067)	5.323(0.006)	2.955(0.108)
1.0	0.8	1.523(0.025)	5.157(0.006)	3.386(0.053)	1.890(0.053)	5.383(0.006)	2.850(0.081)
1.0	0.9	1.607(0.049)	5.197(0.015)	3.236(0.092)	2.020(0.030)	5.437(0.006)	2.692(0.040)
1.0	1.0	1.633(0.032)	5.237(0.006)	3.207(0.061)	2.173(0.040)	5.510(0.000)	2.536(0.047)
1.2	0.1	1.160(0.062)	5.007(0.015)	4.324(0.216)	1.287(0.032)	5.130(0.000)	3.989(0.101)
1.2	0.2	1.247(0.021)	5.037(0.006)	4.041(0.064)	1.350(0.085)	5.170(0.000)	3.840(0.241)
1.2	0.3	1.303(0.047)	5.067(0.006)	3.891(0.145)	1.463(0.032)	5.200(0.000)	3.555(0.077)
1.2	0.4	1.340(0.036)	5.100(0.000)	3.808(0.104)	1.523(0.032)	5.250(0.010)	3.447(0.071)
1.2	0.5	1.440(0.017)	5.130(0.000)	3.563(0.043)	1.577(0.015)	5.287(0.015)	3.353(0.023)
1.2	0.6	1.477(0.006)	5.173(0.006)	3.503(0.012)	1.697(0.040)	5.333(0.015)	3.145(0.080)
1.2	0.7	1.530(0.026)	5.213(0.015)	3.408(0.059)	1.760(0.036)	5.387(0.006)	3.061(0.065)
1.2	0.8	1.587(0.065)	5.267(0.012)	3.323(0.131)	1.883(0.012)	5.443(0.012)	2.890(0.022)
1.2	0.9	1.647(0.071)	5.317(0.006)	3.233(0.138)	1.980(0.035)	5.493(0.015)	2.775(0.048)
1.2	1.0	1.683(0.029)	5.350(0.010)	3.179(0.055)	2.090(0.035)	5.543(0.015)	2.653(0.046)

TABLE XI. Mean and standard deviation (in parenthesis) for the peak vibrational frequencies ν_L and ν_S and ratio ν_S/ν_L [extracted from Eq. (9)] for particles in the contact (L) and first solid (S) layer at the hotter and colder L/S interface for parameter values $(T_{\text{source}}, T_{\text{sink}}) = (1.4, 1.2)$, $\sigma_{LS} = 0.8, 1.0$ and 1.2 and $\varepsilon_{LS} = 0.1, 0.2, \dots, 0.8, 1.0$. All quantities are in reduced units defined in Table I.

σ_{LS}	ε_{LS}	Hotter L/S interface			Colder L/S interface		
		ν_L	ν_S	ν_S/ν_L	ν_L	ν_S	ν_S/ν_L
0.8	0.1	2.397(0.015)	4.960(0.000)	2.070(0.013)	2.390(0.017)	5.010(0.000)	2.096(0.015)
0.8	0.2	1.243(0.006)	4.990(0.000)	4.013(0.019)	1.323(0.023)	5.040(0.000)	3.809(0.066)
0.8	0.3	1.323(0.029)	5.017(0.006)	3.792(0.086)	1.440(0.026)	5.067(0.006)	3.519(0.062)
0.8	0.4	1.390(0.036)	5.037(0.006)	3.625(0.097)	1.450(0.078)	5.093(0.006)	3.519(0.186)
0.8	0.5	1.457(0.038)	5.053(0.006)	3.471(0.085)	1.557(0.032)	5.117(0.006)	3.288(0.065)
0.8	0.6	1.543(0.006)	5.073(0.006)	3.287(0.009)	1.657(0.050)	5.137(0.006)	3.102(0.091)
0.8	0.7	1.577(0.031)	5.100(0.010)	3.236(0.069)	1.663(0.042)	5.167(0.006)	3.108(0.080)
0.8	0.8	1.637(0.040)	5.127(0.006)	3.134(0.077)	1.790(0.035)	5.203(0.006)	2.908(0.052)
0.8	0.9	1.690(0.040)	5.150(0.010)	3.049(0.075)	1.860(0.017)	5.233(0.015)	2.814(0.029)
0.8	1.0	1.753(0.050)	5.177(0.006)	2.954(0.086)	1.940(0.053)	5.273(0.006)	2.719(0.070)
1.0	0.1	1.167(0.032)	5.023(0.012)	4.308(0.127)	1.220(0.062)	5.067(0.006)	4.160(0.205)
1.0	0.2	1.210(0.044)	5.057(0.006)	4.183(0.149)	1.307(0.035)	5.097(0.006)	3.902(0.106)
1.0	0.3	1.287(0.015)	5.073(0.006)	3.943(0.044)	1.367(0.015)	5.123(0.006)	3.749(0.039)
1.0	0.4	1.333(0.046)	5.107(0.006)	3.833(0.138)	1.437(0.006)	5.157(0.006)	3.589(0.010)
1.0	0.5	1.473(0.045)	5.130(0.000)	3.484(0.106)	1.463(0.047)	5.190(0.000)	3.549(0.116)
1.0	0.6	1.500(0.030)	5.160(0.000)	3.441(0.069)	1.573(0.100)	5.227(0.006)	3.331(0.220)
1.0	0.7	1.590(0.036)	5.193(0.006)	3.267(0.072)	1.663(0.029)	5.273(0.012)	3.171(0.059)
1.0	0.8	1.640(0.104)	5.237(0.006)	3.201(0.194)	1.787(0.045)	5.317(0.006)	2.977(0.076)
1.0	0.9	1.657(0.061)	5.283(0.006)	3.192(0.123)	1.860(0.017)	5.363(0.006)	2.884(0.028)
1.0	1.0	1.733(0.023)	5.343(0.012)	3.083(0.038)	1.880(0.036)	5.420(0.017)	2.884(0.064)
1.2	0.1	1.193(0.040)	5.057(0.006)	4.241(0.140)	1.240(0.036)	5.100(0.000)	4.115(0.118)
1.2	0.2	1.250(0.072)	5.087(0.006)	4.078(0.235)	1.323(0.021)	5.120(0.000)	3.870(0.061)
1.2	0.3	1.357(0.015)	5.127(0.012)	3.779(0.051)	1.370(0.046)	5.167(0.012)	3.774(0.127)
1.2	0.4	1.443(0.067)	5.153(0.006)	3.576(0.165)	1.467(0.021)	5.197(0.006)	3.544(0.054)
1.2	0.5	1.493(0.021)	5.193(0.015)	3.478(0.059)	1.560(0.066)	5.243(0.006)	3.365(0.143)
1.2	0.6	1.553(0.032)	5.237(0.006)	3.372(0.067)	1.593(0.021)	5.287(0.012)	3.318(0.039)
1.2	0.7	1.600(0.082)	5.280(0.000)	3.306(0.172)	1.700(0.020)	5.340(0.010)	3.141(0.034)
1.2	0.8	1.690(0.036)	5.333(0.006)	3.157(0.064)	1.787(0.021)	5.400(0.010)	3.023(0.034)
1.2	0.9	1.750(0.046)	5.380(0.000)	3.076(0.081)	1.843(0.070)	5.440(0.000)	2.954(0.113)
1.2	1.0	1.793(0.032)	5.430(0.010)	3.029(0.059)	1.917(0.029)	5.493(0.012)	2.867(0.049)